

---

Masters Theses

Student Theses and Dissertations

---

Summer 1988

## Behavior of reinforced loess specimens under triaxial load

Mohammad Taghi Izadi

Follow this and additional works at: [https://scholarsmine.mst.edu/masters\\_theses](https://scholarsmine.mst.edu/masters_theses)



Part of the [Civil Engineering Commons](#)

Department:

---

### Recommended Citation

Izadi, Mohammad Taghi, "Behavior of reinforced loess specimens under triaxial load" (1988). *Masters Theses*. 598.

[https://scholarsmine.mst.edu/masters\\_theses/598](https://scholarsmine.mst.edu/masters_theses/598)

This thesis is brought to you by Scholars' Mine, a service of the Missouri S&T Library and Learning Resources. This work is protected by U. S. Copyright Law. Unauthorized use including reproduction for redistribution requires the permission of the copyright holder. For more information, please contact [scholarsmine@mst.edu](mailto:scholarsmine@mst.edu).

BEHAVIOR OF REINFORCED LOESS SPECIMENS  
UNDER TRIAXIAL LOAD

BY


MOHAMMAD TAGHII IZADI 1950-


A THESIS

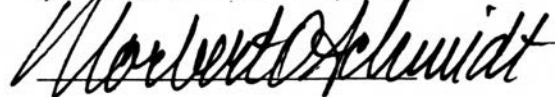
Presented to the Faculty of the Graduate School of the  
UNIVERSITY OF MISSOURI - ROLLA  
In Partial Fulfillment of the Requirements for the Degree  
MASTER OF SCIENCE IN CIVIL ENGINEERING

1988

Approved by

  
\_\_\_\_\_  
Rodney W. Lentz  
(Advisor)

  
\_\_\_\_\_  
Harold Dean Keith

  
\_\_\_\_\_  
Norbert Schmidt

## ABSTRACT

Effects of reinforcement on shear strength of a loessial (silty) soil are studied. Unconsolidated undrained triaxial tests are performed on unreinforced and fabric reinforced soil specimens. Analyses of the test results showed that in general the shear strength of remolded loess specimens were improved substantially and increase in the shear strength was directly related to reinforcement spacing.

The mechanism of soil-reinforcement interaction and several existing analytical models are described. A modified analytical model based on enhanced confining theory is developed. This model can be used in assessing the effects of the reinforcement on shear strength of triaxial specimens. Comparison of the theoretical and the test results shows good agreement between the two.

The problem of non-uniform state of stress and strain within triaxial specimens is also considered, and a new simple model based on the beam-column analogy is developed. This model can be used in calculating the magnitude of normal stress at various points within cylindrical triaxial specimens. Each of the two proposed models is applicable to both unreinforced specimens loaded through non-lubricated end platens and fabric reinforced specimens.

## ACKNOWLEDGMENTS

Praise be to Allah Who taught the man that which he did not know.

The author expresses his appreciation to Dr. Shamsheer Prakash for his continuous guidance throughout the preparation of this research.

I express my thanks to my committee members Dr. Norbert O. Schmidt for his valuable guidance and instructions, Dr. Rodney, W. Lentz for his advice and suggestions, and to Dr. Harold, D. Keith for his valuable time and help.

And finally to my parents, and wife, whose care and support have always been present and will never be forgotten.

## TABLE OF CONTENTS

|  | Page      |
|--|-----------|
| ABSTRACT .....   | ii        |
| ACKNOWLEDGMENTS .....  | iii       |
| LIST OF ILLUSTRATIONS .....  | vi        |
| LIST OF TABLES .....   | vii       |
| <b>I. INTRODUCTION .....</b>   | <b>1</b>  |
| <b>A. GENERAL .....</b>  | <b>1</b>  |
| <b>B. PURPOSE AND SCOPE OF THE INVESTIGATION .....</b>                   | <b>3</b>  |
| <b>II. REVIEW OF LITERATURE .....</b>                                    | <b>5</b>  |
| <b>A. HISTORICAL REVIEW .....</b>  | <b>5</b>  |
| <b>B. MECHANISM OF REINFORCED EARTH-THEORETICAL MODELS .....</b>         | <b>6</b>  |
| 1. Anisotropic Elastic Theory .....                                      | 7         |
| 2. Anisotropic Cohesion Theory .....                                     | 9         |
| 3. Enhanced Confining Pressure Theory .....                              | 12        |
| 4. Forging Theory .....  | 16        |
| 5. Limit Equilibrium Theory .....  | 18        |
| 6. Energy Theory .....   | 20        |
| <b>C. DISCUSSION ON THEORETICAL MODELS .....</b>                         | <b>22</b> |
| <b>D. NON-UNIFORM STRESS DISTRIBUTION .....</b>                          | <b>23</b> |
| <b>E. DISCUSSION ON NON-UNIFORM STRESS AND STRAIN DISTRIBUTION .....</b> | <b>34</b> |
| <b>III. PROPOSED MODELS .....</b>  | <b>36</b> |
| <b>A. ENHANCED CONFINING PRESSURE MODEL .....</b>                        | <b>36</b> |
| 1. Uniform Stress Distribution in Triaxial Specimens .....               | 36        |
| 2. The Model .....   | 37        |
| <b>B. BEAM-COLUMN MODEL .....</b>  | <b>40</b> |
| <b>C. STATE OF STRESS AT FAILURE .....</b>                               | <b>43</b> |

|     |   |    |
|-----|---|----|
| D.  | EFFECTS OF ASPECT RATIO ON STRENGTH .....                             | 43 |
| IV. | TESTS RESULTS AND DISCUSSION .....                                    | 46 |
| A.  | PROCEDURES AND TEST DATA .....  | 46 |
| 1.  | Reinforcing Material .....  | 46 |
| 2.  | Compaction .....  | 47 |
| 3.  | Specimen Preparation .....  | 48 |
| 4.  | Triaxial Testing .....  | 49 |
| 5.  | Phase-one Unreinforced Specimens .....                                | 49 |
| 6.  | Phase-Two Reinforced Specimens .....                                  | 49 |
| B.  | TEST DATA .....   | 50 |
| C.  | ANALYSIS OF TESTS RESULTS .....                                       | 54 |
| 1.  | Failure Strength .....  | 54 |
| a.  | Interpretation of Test Results with Enhanced Confining Theory .....   | 54 |
| b.  | Interpretation of Test Results with Enhanced Cohesion Theory .....    | 55 |
| 2.  | Effects of Moisture Content on Strength of Reinforced Specimens ..... | 55 |
| 3.  | Effects of Aspect Ratio on Strength of Reinforced Specimens .....     | 57 |
| D.  | EFFECT OF REINFORCEMENT ON MODULUS .....                              | 57 |
| 1.  | Tangent Modulus .....   | 57 |
| 2.  | Secant Modulus at 50 Percent of Failure Stress .....                  | 57 |
| 3.  | Secant Modulus at 50 Percent of Failure Strain .....                  | 57 |
| E.  | DISCUSSION .....  | 59 |
| 1.  | Comparison of Tests Results With Enhanced Confining Theory. . .       | 60 |
| 2.  | Effects of Non-uniform Stress Distribution .....                      | 61 |
| F.  | COMPARISON OF THE BEAM-COLUMN MODEL WITH EXPERIMENTAL DATA .....      | 62 |
| V.  | CONCLUSIONS .....   | 79 |
|     | REFERENCES .....  | 81 |
|     | VITA .....  | 88 |

## LIST OF ILLUSTRATIONS

| Figure |   | Page |
|--------|---|------|
| 1      | Munster's reinforced retaining wall. ....   | 6    |
| 2      | Vidal's Sand Pile: (a). unreinforced, (b) reinforced. ....  | 7    |
| 3      | Reinforcement induced cohesion, (after Long, 1972). ....  | 10   |
| 4      | Coulomb analysis for reinforced specimen. ....  | 11   |
| 5      | Comparison of theoretical and experimental results, (after Schlosser and Long, 1973). ....  | 13   |
| 6      | Enhanced confining pressure interpretation. ....  | 13   |
| 7      | Variation of strength with aspect ratio, (after Yang, 1972). ....   | 15   |
| 8      | Enhanced confining pressure. ....   | 15   |
| 9      | Stress on cylindrical element. ....   | 17   |
| 10     | Comparison of theoretical and test data, (after Ingold, 1980). ....   | 17   |
| 11     | Stress in shear box. ....   | 19   |
| 12     | Energy relationship. ....   | 21   |
| 13     | Observed and theoretical maximum tie tension, (after Osman, 1979). ....   | 23   |
| 14     | Comparison of stress distribution by different methods at the end surface, for perfectly confined ends. ....                              | 26   |
| 15     | Section of a polished steel specimen compressed to 56% of its height, (after Mercall, Papimo and McLaughlin, 1983). ....                  | 28   |
| 16     | Variation of normal stress at mid-height, (after Shockley and Ahlvin, 1960). ...  | 28   |
| 17     | Density variation in saturated sand specimen, (after Shockley and Ahlvin, 1960). ....   | 29   |
| 18     | Density profile in triaxial specimens, (after Bouvard and Stutz, 1986). ....  | 29   |
| 19     | Dilation zone. ....   | 31   |
| 20     | Influence of aspect ratio on shear strength of specimens with various degrees of end restraint, (after Bishop and Green, 1965). ....      | 32   |
| 21     | Pore pressure distribution at the end and mid-height of specimens with fixed ends and free ends, (after Barden and McDermott, 1965). .... | 33   |
| 22     | Distribution of axial strain in specimen with rough ends, (after Kirkpatrick and Younger). ....   | 33   |
| 23     | Rigid end zones in triaxial specimen loaded through rough end platens, (after Kirkpatrick and Younger, 1970). ....                        | 34   |

## Illustration continued

|    |   |    |
|----|---|----|
| 24 | Homogeneous state of stress in triaxial specimen. ....  | 37 |
| 25 | Stress acting on a triaxial specimen loaded through rough surfaces. ....  | 38 |
| 26 | Cylindrical specimen composed of n sections. ....   | 40 |
| 27 | Stress acting at each section of specimen. ....   | 41 |
| 28 | Free-body diagram of a section. ....  | 42 |
| 29 | Normal stress distribution at the end and mid-height of a triaxial specimen loaded through rough surfaces. ....   | 44 |
| 30 | Mohr-Coulomb failure envelope for points A and B. ....  | 45 |
| 31 | Mohr-Coulomb failure envelope for points C and D. ....  | 45 |
| 32 | Compaction curve. ....  | 65 |
| 33 | Stress-strain relationship for unreinforced specimens. Tests No. 1, 2 & 3 at 12% moisture content and tests No. 4, 5 & 6 at 17% moisture content. ....          | 66 |
| 34 | Stress-strain relationship for reinforced specimens with aspect ratio of 0.4 and 12% moisture content. Tests No. 7, 8 & 9, compared with Tests No. 1-3. ....    | 67 |
| 35 | Stress-strain relationship for reinforced specimens with aspect ratio of 0.4 and 17% moisture content. Tests No. 10, 11 & 12, compared with tests No. 4-6. ...  | 68 |
| 36 | Stress-strain relationship for reinforced specimens with aspect ratio of 0.5 and 17% moisture content. Tests No. 13, 14 & 15, compared with tests No. 4-6. ...  | 69 |
| 37 | Stress-strain relationship for reinforced specimens with aspect ratio of 0.67 and 17% moisture content. Tests No. 16, 17 & 18, compared with tests No. 4-6. ... | 70 |
| 38 | Comparison of stress-strain curves for 3 pairs of identical tests. No. 15, 20, 21, 22 & 23. ....  | 71 |
| 39 | Mohr-Coulomb failure envelope for unreinforced specimens with 12% moisture content, tests No. 1-3. ....   | 72 |
| 40 | Mohr-Coulomb failure envelope for unreinforced specimens with 17% moisture content, tests No. 4-6. ....   | 72 |
| 41 | Mohr-Coulomb failure envelope for tests No. 7-9, using the enhanced confining pressure theory, compared with tests No. 1-3. ....                                | 73 |
| 42 | Mohr-Coulomb failure envelope for tests No. 10-12, using the enhanced confining pressure theory, compared with tests No. 4-6. ....                              | 73 |
| 43 | Mohr-Coulomb failure envelope for Tests No. 13-15, using the enhanced confining pressure theory. ....   | 74 |
| 44 | Mohr-Coulomb failure envelope for tests No. 16-18, using the enhanced confining pressure theory. ....   | 74 |



## Illustration continued

|    |   |    |
|----|---|----|
| 45 | Mohr-Coulomb failure envelope for tests No. 7-9, using enhanced cohesion theory. ....                                 | 75 |
| 46 | Mohr-Coulomb failure envelope for tests No.10-12, using enhanced cohesion theory. ....                                | 75 |
| 47 | Comparison of the experimental with theoretical results based on the enhanced confining pressure theory. ....         | 76 |
| 48 | Comparison of the experimental with theoretical (b) for aspect ratios $> 0.67$ . .                                    | 77 |
| 49 | Variation of bond stress angle along radius. ....   | 77 |
| 50 | Comparison of experimental and theoretical values of normal stress: a- across the mid-height, b- across the end. .... | 78 |

## LIST OF TABLES

| Table |  | Page |
|-------|--|------|
| I     | INDEX PROPERTIES OF LOESS .....                                  | 47   |
| II    | PROPERTIES OF GEOTEXTILE FABRIC GTF-200. ....                    | 48   |
| III   | TRIAXIAL TEST RESULTS (UNREINFORCED SPECIMENS) .....             | 51   |
| IV    | TRIAXIAL TEST RESULTS (REINFORCED SPECIMENS) .....               | 52   |
| V     | VALUES OF ENHANCED CONFINING PRESSURE FROM TEST<br>RESULTS ..... | 56   |
| VI    | VALUES OF TANGENT AND SECANT MODULUS .....                       | 58   |
| VII   | THEORETICAL STRENGTH BASED ON ENHANCED CONFINING<br>THEORY ..... | 64   |

## I. INTRODUCTION

### A. GENERAL

In general loads applied to an earth structure are compressive in nature. The application of compressive force in one direction results in expansion of the soil mass in the other orthogonal directions. Soils can withstand compression but are weak in tension. This weakness was noticed by the early builders who developed various techniques in order to overcome this problem. Reinforcing of soils by use of tensile resisting materials is one such technique and its basic principle was first abundantly demonstrated in nature by animals, birds and the action of tree roots. Man used this principle in construction of mud walls, roads, earth dams, and foundations by use of fibers, straps, bars or timbers in combination with soil. However with a few exceptions, such as the effect of straw on unfired clay bricks, the concept of reinforced earth was not explained, popularized, and practiced until the work of Henri Vidal (1966). He systematically demonstrated the wide applications of reinforced earth and developed design procedures which caught the attention of engineers throughout the world.

In the past two decades, it has been demonstrated that in many circumstances reinforced earth structures are more economical than their alternative structures. In general, these structures have been built using granular material containing less than 25 percent passing the number 200 sieve and having a plasticity index smaller than 6. This is not altogether surprising as the bond between the reinforcing material and the soil is best achieved by using such soils. However, this criterion has limited the application of reinforced earth in areas where the residual soils are fine grained materials and a fill of such quality is not economically available. On the other hand, fine grained soils present difficulties associated with poor drainage, slow development of effective stress, low friction angle, corrosion and time dependent deformations. Schlosser and Vidal (1969) concluded that in the case of fine grained materials, even if the shear stress is fully mobilized, the maximum possible short term bond stress that could develop would be equal to the undrained shear strength of the soil. This is generally low compared to the bond stress developed by the granular backfill normally used in practice, Ingold (1980).

The successful application of fine grained soils in reinforced earth structures may lead to significant savings in construction costs in areas where granular materials of such quality are not available. This aspect led to several investigations on the use of fine grained soils in reinforced earth especially in the United Kingdom. For example Ingold (1978, 1980, 1981, 1982) extensively studied the effects of reinforcement on strength properties of clay, and Murray and Boden (1979) investigated the performance of a 6m. high reinforced embankment built with cohesive soils. The latter study demonstrated practicability of short term construction of reinforced earth walls with cohesive materials. A further example is that of Jewell and Janes (1981) who investigated the feasibility of using cohesive soils and coal mine waste as backfill materials in reinforced earth structures. The laboratory and field tests showed that both materials could be used effectively in construction of reinforced earth structures.

In general, most of the laboratory investigations on reinforced fine grained soils have been performed on reinforced triaxial and/or direct shear specimens. However, it has been known for more than one century that the state of stress and strain within triaxial specimen is non-uniform when it is loaded through non-lubricated surfaces. Further, the similarity of stress distribution in unreinforced and reinforced specimens was pointed out by Ingold (1980). Analyses based on elastic theory have shown that non-uniform stress distribution can have significant effects on the shear strength of triaxial specimens, Filon (1902), Pickett (1944), D'Appolonia and Newmark (1951), Balla (1957, 1960), Bishop and Green (1965) and others.

In the case of unreinforced specimens, effects of end restraint on shear strength can be minimized either by lubricating the end platens, or else by using an appropriate aspect ratio (height to diameter ratio). Theoretically the aspect ratio should be selected such that a non-lubricated specimen fails under the same normal stress as a comparable lubricated specimen. However, in practice most of the triaxial tests are performed on specimens with aspect ratios of 2. On the other hand, in reinforced specimens, reinforcing effects are derived from the restraining effects of reinforcing material at the soil-reinforcement interface which is destroyed upon lubrication. One way of minimizing non-uniformity in the state of stress and strain is to perform tests on triaxial specimens with small aspect ratios. However, in order to investigate the possible effects of reinforcement spacing on shear strength of specimens it is also

necessary to test specimens with large aspect ratios, but increase of the aspect ratio is accompanied by an increase in the non-uniformity of state of stress and strain within the specimen.

Moreover, theoretical investigations had led to the development of a number of analytical models which have been used in determining the effects of reinforcement on strength properties of the soils. However, none of these models consider the effects of non-uniform stress distribution on the test results.

## **B. PURPOSE AND SCOPE OF THE INVESTIGATION**

The primary objective of this investigation is to use laboratory test results and theoretical analysis to assess the feasibility of using loessial (silty) soils in reinforced earth structures. Also, the effects of non-uniform stress distribution on shear strength of reinforced as well as unreinforced cylindrical soil specimens subjected to triaxial compression force are considered.

Loess occupies the uppermost stratigraphic position over extensive areas of the central United States. About 17% of Europe is covered by loess, including parts of France, Germany, and eastern Europe. It also covers large areas of Russia, Siberia and China. It is found in the plains regions of Argentina and Uruguay and parts of New Zealand. It is a uniform cohesive wind-blown sediment, commonly light brown in color. The size of most of the particles ranges between the narrow limits of 0.01 and 0.05 mm. The cohesion is due to the presence of a binder that may be predominantly calcareous or clayey, (Terzaghi and Peck, 1948)

However despite the wide occurrence of loess, its feasibility as a potential backfill material in reinforced earth structures has not been studied. Indeed some of the problems associated with the use of fine grained soils, i.e. drainage, development of effective stress, and corrosion may decrease by use of this soil.

Hence, it has been decided to study the effects of reinforcement on behavior of reinforced loess specimens under triaxial compression loads. In order to minimize the number of variables, the investigation is confined to the effects of a woven geotextile fabric on shear strength of

partially saturated and remolded loess. Effects of moisture content and reinforcement spacing are also studied. Special attention is given to effects of non-uniform stress distribution on triaxial test results. Two models are developed. The first model uses the enhanced confining pressure theory to predict the shear strength of reinforced specimens. The second model is developed by using the beam-column analogy and can be used in estimating the magnitude of normal stress at various points within unreinforced and reinforced triaxial specimens.

## II. REVIEW OF LITERATURE

### A. HISTORICAL REVIEW

It has been said that there is nothing new under the sun, and today's techniques and discoveries have already been created in nature by the Creator. In the case of reinforced earth, nature has pointed the way in the home building techniques of some members of the animal kingdom who make nests from combination of mud and straw. Early builders used the idea in adobe construction and subsequently throughout the ages up to recent times in walls and foundations.

As far back as the fifth millennium B. C., compacted clay with reeds were used in the construction of the crude mud huts in Sialk on the Iranian Plateau. In the Far East, for thousands of years it has been the practice to reinforce large earth structures with reeds, rushes or bamboos, (Ingold, 1980). One of the earliest example of reinforced earth in existence is the Ziggurat of the ancient city Dur-Kurigalzu now known as Aguar-Quf, constructed of clay and sand, with reeds for reinforcement. At present 148ft. (45m.) high, it is believed to have stood 285ft. (87m.) high when originally constructed in 1500 B. C., (Jones, 1978). The oldest historical example of the use of fabric as an aid to road construction over soft ground include use of woven reed mats by ancient Romans. In a style remarkably similar to our present-day techniques, they would lay mats over marshy ground before overlaying with stones, (Rankilor, 1981).

In the last century, Pasley (1822) introduced reinforced earth for military construction in the British Army. He used layers of brushwood twigs, wooden planks or sheets of canvas as the reinforcing media, (Rankilor, 1981). A significant development to the modern concept of reinforced earth was made in the United States by Munster (1925). He built an earth retaining wall using arrays of wooden reinforcing members and a light facing. Munster minimized the problem associated with the settling of the backfill by using sliding attachments between the reinforcing members and the facing, Fig. 1, (Jones, 1978). In 1957 Lallemand advocated the use

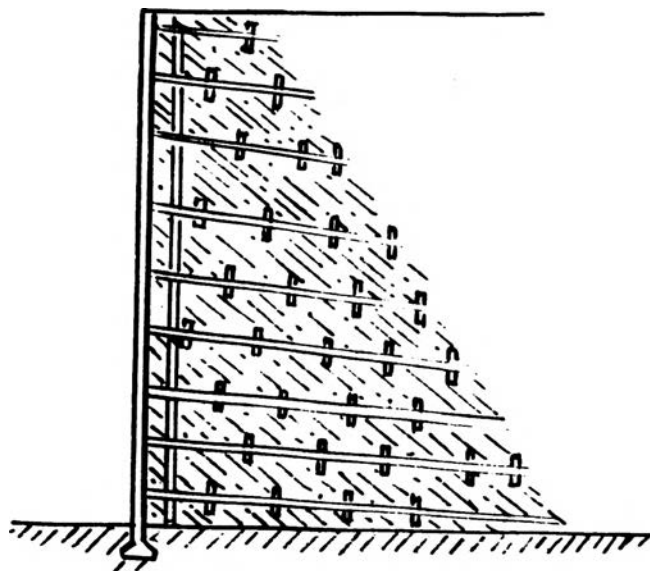


Figure 1. Munster's reinforced retaining wall.

of a prismatic reinforcing member to which the plates of various shapes were attached to increase the pull-out resistance of the reinforcement, (Ingold, 1980).

What might be regarded as the first credible reinforcing system was introduced in France by Henri Vidal on 1963. The first major reinforced earth structure was built on the Autoroute de Menton in 1968, since which reinforced earth has been used in retaining walls, railways, bridge abutments, slabs, earth dams, slope stabilization, and foundations throughout the world.

## **B. MECHANISM OF REINFORCED EARTH-THEORETICAL MODELS**

Natural stratification of alternate horizontal layers of soft and stiff soils are probably the first reinforced earth systems. This was recognized only some forty years ago by A. Casagrande, who pointed out its importance in engineering of the foundations. More recently, Henri Vidal (1966) found that the slope of a pile of sand can be made steeper by addition of horizontal layers of pine needles, Fig. 2. Vidal's basic conclusion was that when dry soil is combined with a rough tensile resisting material, the resulting composite material is stronger than the soil.



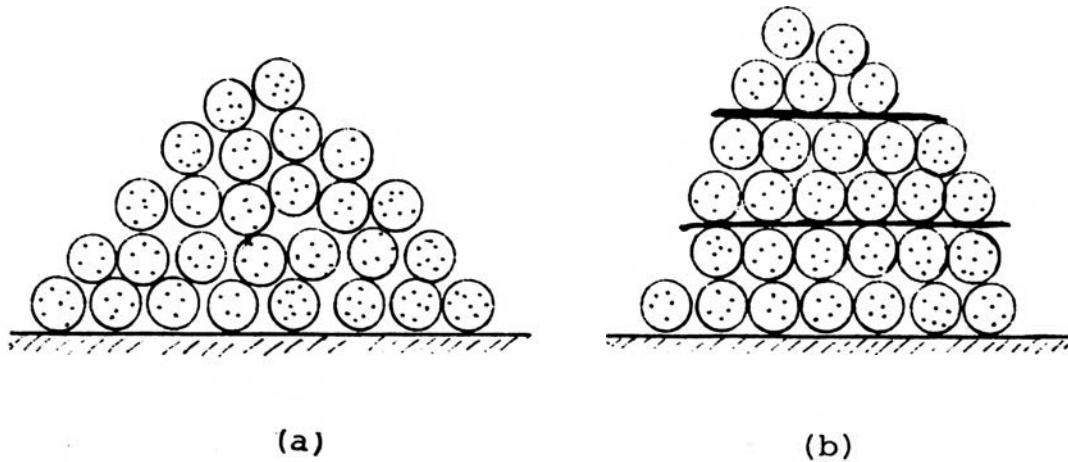


Figure 2. Vidal's Sand Pile, a) unreinforced, b) reinforced.

In the past two decades many researchers have studied the behavior of soil-reinforcement systems and proposed several theoretical and analytical models which are being used in the design of various types of reinforced earth structures. Several of these models are described in the following sections.

1. Anisotropic Elastic Theory. In foundations over the stratified soils, the strong layers may reinforce the soft layers and therefore act as an additional confinement for the soft soil which is not determined by theory of the isotropic elasticity. Westergaard (1938) investigated this problem and assumed that the layer of soft soil could be modeled as an elastic material (the Westergaard material) and the layer of strong soil as closely spaced sheets of flexible but inextensible material of negligible thickness, which prevents lateral strain of the composite material. He assumed further that:

- a. There is no slip between layers of soft material and the stiff sheets.
- b. Both layers are isotropic, and horizontal.
- c. Horizontal stresses are principal stresses.

Further by application of isotropic elastic theory he derived a simple expression for horizontal strain as:

$$\epsilon_h = \frac{\sigma_{1r}(1 - \nu) - \nu\sigma_3}{E} \quad (2.1)$$

where:  $\epsilon_h$  = horizontal strain

$\sigma_{1r}$  = vertical stress

$\sigma_3$  = horizontal stress

E = Young's modulus

$\nu$  = Poisson's ratio

Since strain in the horizontal direction is prevented,  $\epsilon_h$  is equal to zero and equation 2.1 can be simplified to:

$$\frac{\sigma_3}{\sigma_{1r}} = \frac{\nu}{(1 - \nu)} \quad (2.2)$$

Further advances of the above were made by several investigators. Wordle and Gerrard (1972) studied the properties of a layered system in which the relative stiffness and thickness of the layers were of intermediate magnitude. Harrison and Gerrard (1972) considered a general case of a finite range of values of stiffness and thickness of the reinforced layers. They related the elastic properties of the equivalent homogeneous material, E and  $\nu$ , to properties of the separate layers,  $E_1, \nu_1$  and  $E_2, \nu_2$ . Harmann and Al-Yassin (1978) used both composite and discrete approaches and considered slippage and yielding of the reinforcement with nonlinear behavior of the soil. Gerrard (1981) proposed a composite model for analyzing a reinforcing system of parallel, equally spaced planes. In his analysis the stress-deformation properties of the reinforced soil system were described in terms of an equivalent homogeneous cross-anisotropic material.

The above analyses are primarily concerned with the overall response of layered structures, which models them as an equivalent homogeneous, cross-anisotropic continuum material. The main draw back of the models based on the above theory is that they are limited to analysis of two and three dimensional systems with large number of layers, and small deformations.

2. Anisotropic Cohesion Theory. Long, Guegan, and Legcay (1972) performed a series of triaxial compression tests on dry sand specimens, 100mm. in diameter, and aspect ratios of 2 and 3. Reinforcement was introduced to the specimens in the form of 100mm. diameter discs of 18m $\mu$  thick aluminum foil, which were placed horizontally in the soil specimens. The effect of reinforcement spacing  $h$  as well as the effect of reinforcement tensile strength  $T$  were examined by varying the reinforcement spacing and number of reinforcing discs used to form each layer. Test results showed that above a certain threshold value of applied confining pressure there was a constant increase  $\Delta\sigma_1$  in the applied normal stress at failure, for a given reinforcement tensile strength and spacing, Fig. 3. They concluded that since the failure envelopes were parallel for both the reinforced and the unreinforced specimens, the angle of shearing resistance is the same for both cases and the additional strength could be represented by an apparent anisotropic cohesion  $c$ .

Schlosser and Long (1973) formulated an expression for this pseudo cohesion by considering the failure envelope of a reinforced soil specimen as:

$$\sigma_{1r} = K_p\sigma_3 + \Delta\sigma_1 \quad (2.3)$$

where:  $\sigma_{1r}$  = normal stress for reinforced specimen

$\sigma_3$  = confining pressure

$\Delta\sigma_1$  = increase in strength caused by reinforcement

$K_p$  = coefficient of passive pressure

By comparison of the above expression with the Rankine equation for a  $c - \phi$  soil, we can write:

$$\sigma_1 = K_p\sigma_3 + 2c\sqrt{K_p} \quad (2.4)$$

Equations 2.3 and 2.4 lead to:

$$c = \frac{\Delta\sigma_1}{2\sqrt{K_p}} \quad (2.5)$$

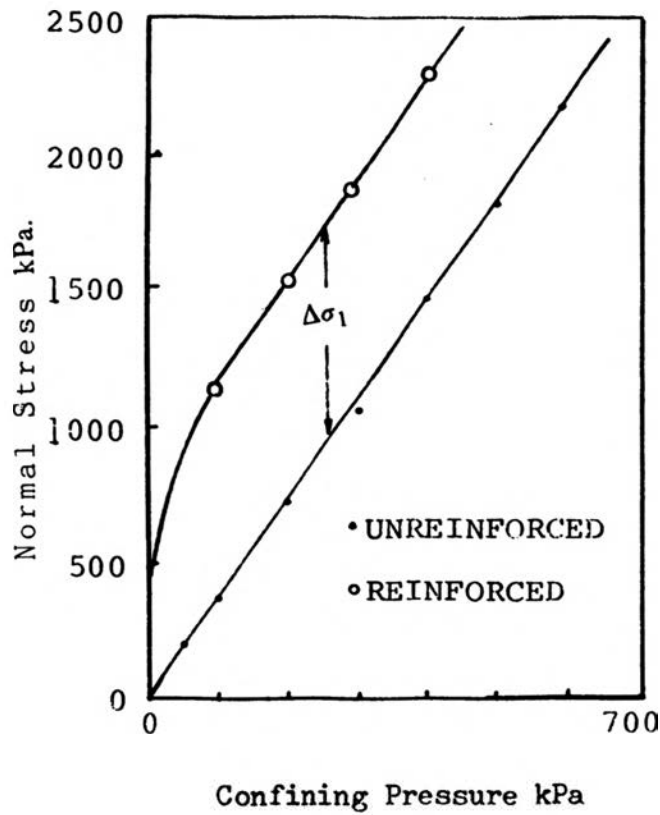


Figure 3. Reinforcement induced cohesion. (after Long, 1972)

Further, they proposed an analytical procedure to determine  $c$  directly from the tensile strength of the reinforcing material. The equilibrium of a reinforced cylinder of soil subjected to axisymmetric loading, cut by a failure plane inclined at  $\alpha$  to the horizontal was considered, Fig. 4. In addition to the resultant force generated by the principal stress  $\sigma_1$ , and  $\sigma_3$ , there is a tensile force  $F$  developed by reinforcement which acts on the failure plane. If the cross-sectional area of the cylindrical section is  $A$ , it follows from the triangle of forces that:

$$\tan(\alpha - \phi) = \frac{H}{\sigma_1 r A} \quad (2.6)$$

where:

$$H = F + \sigma_3 A \tan \alpha \quad (2.7)$$

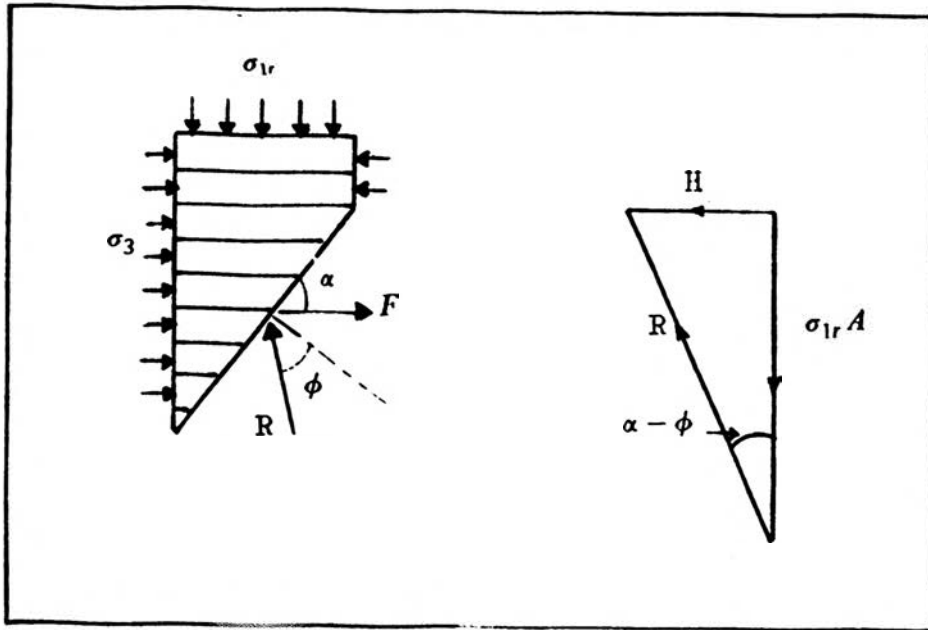


Figure 4. Coulomb analysis for reinforced specimen

From 2.6 and 2.7 we have:

$$F + \sigma_3 A \tan \alpha = \sigma_{1r} A \tan(\alpha - \phi) \quad (2.8)$$

When the specimen is failed by breaking of the reinforcement the tensile force  $F$  is equal to the sum of tensile forces  $T$  from each reinforcement cut by the failure plane. If the vertical spacing of reinforcement  $h$  is small compared to the height of the specimen, then we can write.

$$F = \frac{A \tan \alpha}{h} T \quad (2.9)$$

Combining 2.8 and 2.9 leads to:

$$\sigma_{1r} = (\sigma_3 + T/h) \tan \alpha \cot(\alpha - \phi) \quad (2.10)$$

Maximum value of  $\sigma_{1r}$  occurs when  $\alpha = 45 + \phi/2$ . For this value equation 2.10 reduces to:

$$\sigma_{1r} = K_p \sigma_3 + K_p T/h \quad (2.11)$$

Comparison of 2.3 and 2.11 leads to:

$$\Delta\sigma_1 = K_p \frac{T}{h} \quad (2.12)$$

Subsequent substitution of 2.12 into 2.4 leads to an expression for anisotropic cohesion as:

$$c = \frac{T}{h} \frac{\sqrt{K_p}}{2} \quad (2.13)$$

Comparison of the theory and the experimental results obtained by Schlosser and Long (1973) showed good agreement between the two, Fig. 5.

Later, Hausmann (1976), developed two analytical models, Sigma and Tau, both dealing with bond and tensile failure. The Sigma model assumes that the reinforcement assists the soil to resist lateral expansion. In the Tau model the reinforcement is assumed to introduce horizontal and vertical shear stress into the initially geostatic stress conditions. Hausmann tested his theories by conducting a series of tests on unreinforced and reinforced specimens 70mm in diameter. Test results for specimens failing by rupture of the reinforcement did not show good agreement with the theory. Conversely specimens failing by bond showed quite reasonable agreement with the theory, once a "suitable" value for reinforcement efficiency was chosen.

3. Enhanced Confining Pressure Theory. Consider an unreinforced specimen subjected to triaxial compression stresses. If the end platens are lubricated the applied cell pressure equals the minor principal stress  $\sigma_3$ . The specimen fails under a normal principal stress  $\sigma_1$  and the resulting stress circle is tangential to the failure envelope. On the other hand, when a reinforced specimen is tested at the same applied cell pressure it fails at a higher normal stress  $\sigma_{1r}$ . By assuming that the applied cell pressure is equal to the minor principal stress, the resulting stress circle passes through  $(\sigma_3, \sigma_{1r})$  Fig. 6, and consequently falls outside the failure envelope. Conversely, Yang (1972) assumed that the specimen failed at a constant effective stress ratio, i. e.  $K_e = \frac{\sigma_{3r}}{\sigma_{1r}}$ , in which the value of  $K_e$  is deduced from conventional tests. The stress circle is drawn tangential to the unreinforced specimens failure envelope and the circle intersects the horizontal axis at  $\sigma_{3r} = \sigma_3 + \Delta\sigma_3$ .

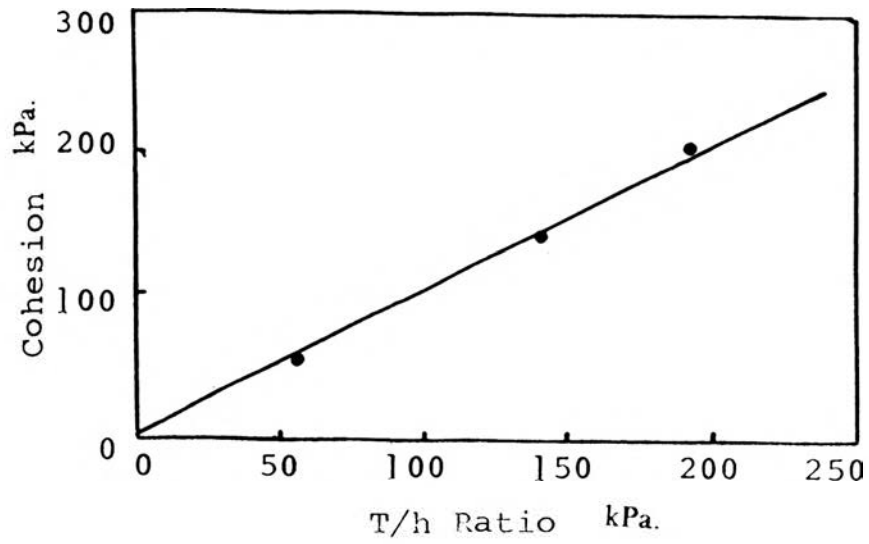


Figure 5. Comparison of theoretical and experimental results, (after Schlosser and Long, 1973).

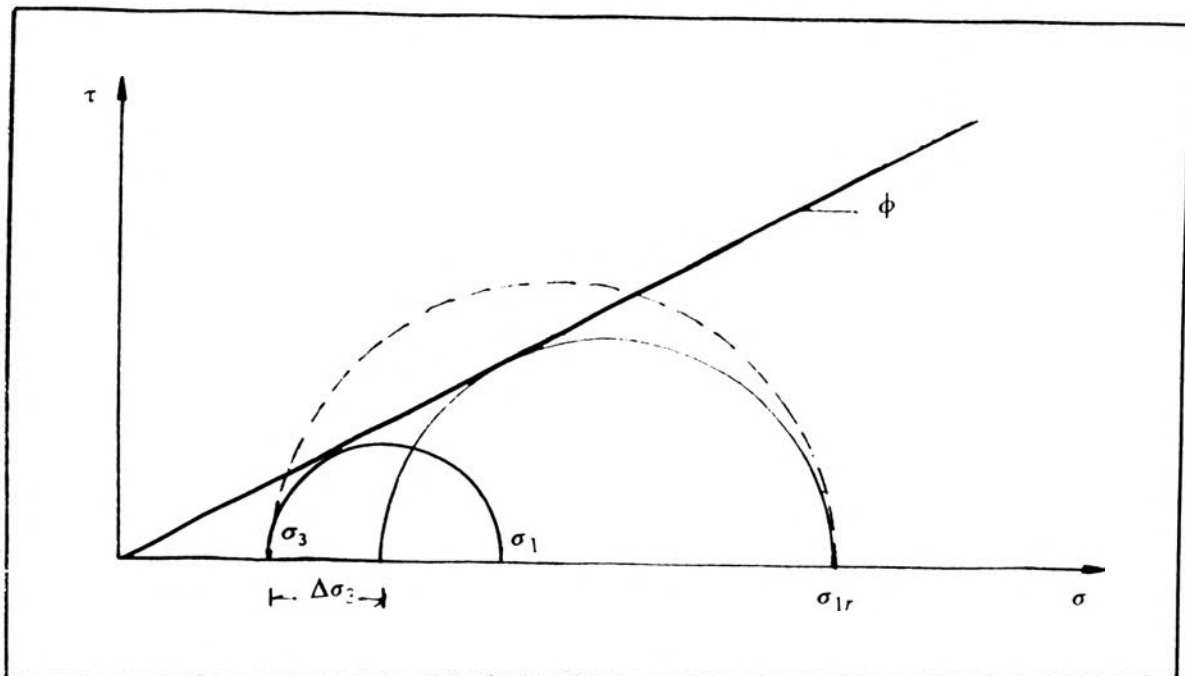


Figure 6. Enhanced confining pressure interpretation.

On this basis, Yang concluded that any increase in the normal stress at failure in the reinforced specimen is due to an enhanced confining pressure  $\Delta\sigma_3$ , Fig. 6. Therefore, for an applied confining pressure  $\sigma_3$  we have:

$$\sigma_{1r} = K_p\sigma_3 + K_p\Delta\sigma_3 \quad (2.14)$$

From which:

$$\Delta\sigma_3 = K_a\sigma_{1r} - \sigma_3 \quad (2.15)$$

Yang (1972), further investigated soil reinforcement bond failure at the soil-reinforcement interface by conducting triaxial compression tests on 2.8 in. diameter sand specimens with aspect ratios of 0.29 to 2.28. The specimens were mounted using heavy steel end platens, which acted as infinitely rigid reinforcing discs. Test results showed a consistent increase in the compressive strength of the specimens as lower aspect ratios were used. A plot of the experimental values of strength ratios, defined as enhanced confining pressures divided by the applied confining pressure,  $(\sigma_3 + \Delta\sigma_3)/\sigma_3$ , against aspect ratios ( $h/d$ ) is shown in Fig. 7. In this figure the solid line has been drawn based on the observed experimental values.

Chapuis (1972) observed that within a reinforced specimen the minor principal stress  $\sigma_{3r}$ , was higher than the applied cell pressure  $\sigma_3$ . In fact  $\sigma_3$  was increased by  $\Delta\sigma_3$  which is derived by inspection of Fig. 8, as:

$$\Delta\sigma_3 = \frac{A\sigma}{Bh} = \frac{T}{h} \quad (2.16)$$

where:  $A$  = area of reinforcement

$B$  = width of specimen

$h$  = height of specimen

$\sigma$  = tensile stress in reinforcement

$T$  = tensile force per unit length =  $A \frac{\sigma}{B}$



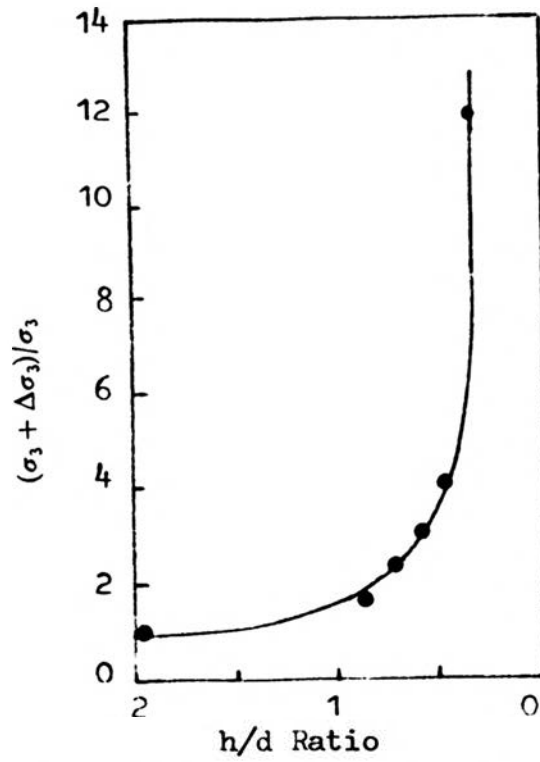


Figure 7. Variation of strength with aspect ratio, (after Yang, 1972).

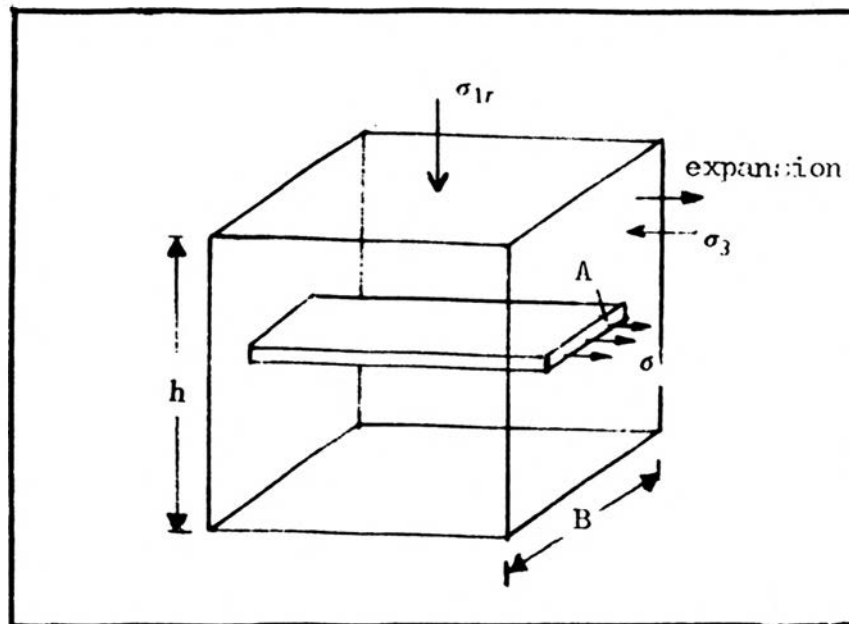


Figure 8. Enhanced confining pressure.

4. **Forging Theory.** The classical forging theory considers the loading of a thick disc of material undergoing compression between rigid frictional platens. Ingold (1978, 1980) applied this theory to reinforced soil specimens subjected to triaxial compression loads. He considered the radial equilibrium of a disc of material of radius  $R$  and thickness  $h$  compressed between two platens, Fig. 9, and assumed that:

- a. The developed shear stresses  $\tau$  are small.
- b. The radial and the circumferential stress components  $\sigma_r$  and  $\sigma_\phi$  are equal and both are principal stresses.
- c. The relative radial strain is a linear function of radial distance from the center of the specimen where the strain is assumed zero.

Then using numerical analysis he proposed an approximate solution for computing the average value of  $(\sigma_{3r}/\sigma_3)$ , as:

$$\left(\frac{\sigma_{3r}}{\sigma_3}\right) = \frac{h K_a}{R \tan \delta} \left[ \exp\left(\frac{R \tan \delta}{h K_a}\right) - 1 \right] \quad (2.17)$$

where:  $\sigma_{3r}$  = enhanced confining pressure

$\delta$  = angle of bond stress

$R$  = disc radius

$K_a$  = coefficient of active earth pressure

$h$  = height of disc

Comparison of the test results with the theoretical values obtained from equation 2.17 showed good agreement when the aspect ratios of the specimens were less than 0.8, Fig. 10.

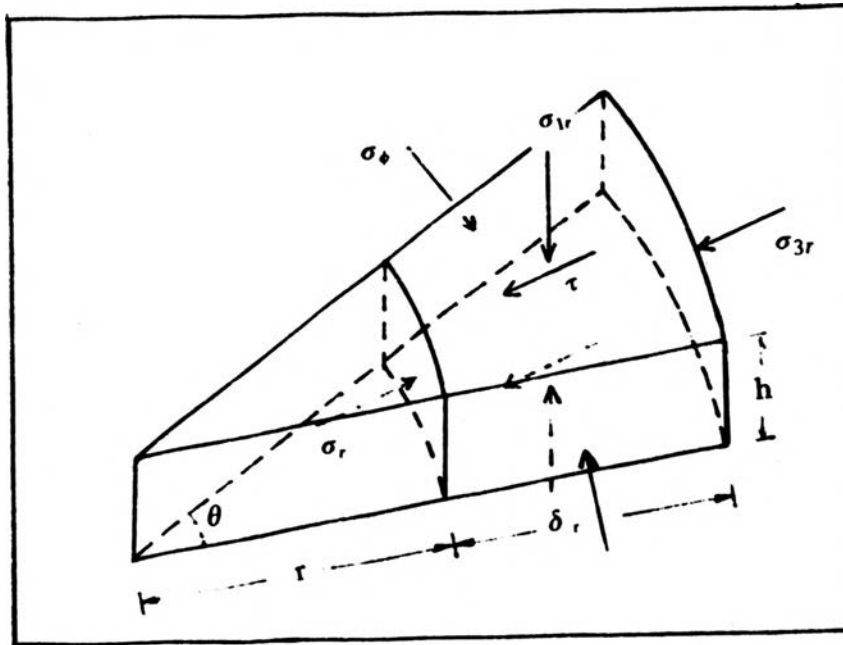


Figure 9. Stress on cylindrical element.

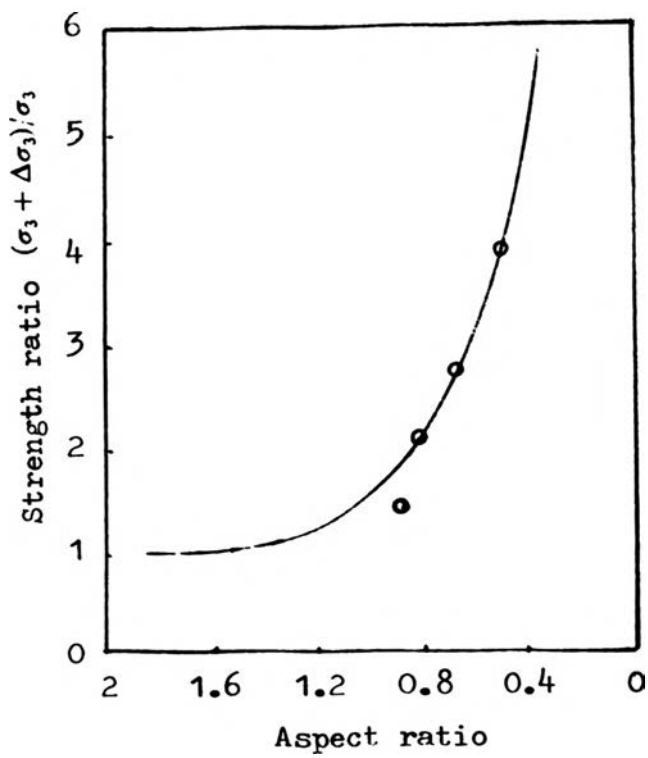


Figure 10. Comparison of theoretical and test data. (after Ingold, 1980).

5. **Limit Equilibrium Theory.** In a limit equilibrium stability analysis, the stress resultants which act on an assumed failure surface are estimated, and compared to the available strength of the soil to provide a measure of stability.

Jewell (1980), considered the equilibrium of a specimen in the direct shear box, taking the central horizontal plane as the potential failure plane, Fig. 11. The soil (sand) contained a single plane of grid reinforcement at an angle  $\theta$  with the vertical, carrying a force at the central plane  $P_{rm}$  per unit depth of the soil. By resolving the total applied load on the horizontal plane into two components  $\sigma_v$  and  $\tau_h$ , the overall stress resultants in the soil on this plane can be expressed as:

$$\tau_{hp} = \tau_h - \frac{P_{rm} \sin \theta}{A_s} \quad (2.18)$$

and

$$\sigma_{hp} = \sigma_v + \frac{P_{rm} \cos \theta}{A_s} \quad (2.19)$$

where:  $A_s$  = cross-sectional area of the slice

Therefore the reinforcement has had two effects, it has reduced the average shear stress  $\tau_{hp}$  carried by the soil, and increased the average normal stress  $\sigma_{hp}$ . Further, for the shear displacement to occur on the horizontal plane we should have:

$$\frac{\tau_{hp}}{\sigma_{hp}} = \tan \phi \quad (2.20)$$

By combining 2.18, 2.19, and 2.20, and rearranging the terms, we get:

$$\frac{\tau_h}{\sigma_v} = \tan \phi + \frac{P_{rm} \cos \theta \tan \phi}{A_s \sigma_v} + \frac{P_{rm} \sin \theta}{A_s \sigma_v} \quad (2.21)$$

Jewell further assumed that the shear stress sustained by the soil alone  $\tau_s$  and the increase in shear strength resulting from the reinforcement in combination with the soil  $\tau_{ext}$  may be considered separately.

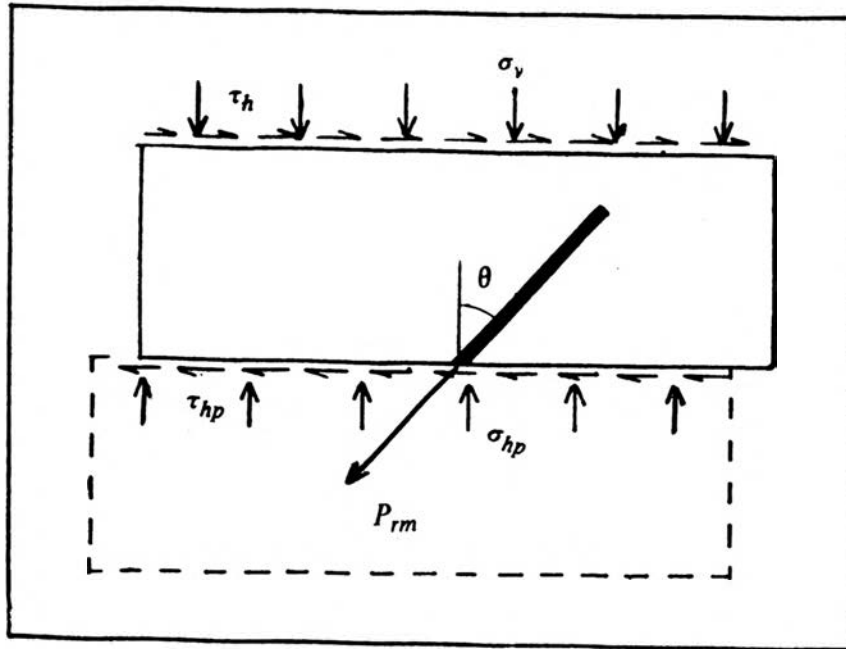


Figure 11. Stress in shear box

Thus:

$$\frac{\tau_h}{\sigma_v} = \frac{\tau_s}{\sigma_v} + \frac{\tau_{ext}}{\sigma_v} \quad (2.22)$$

Where:

$$\tau_s = \sigma_v \tan \phi \quad (2.23)$$

Using 2.21, 2.22 and 2.23 and rearranging the terms we can write:

$$\frac{\tau_{ext}}{\sigma_v} = \frac{P_{rm}}{A_s \sigma_v} (\cos \theta \tan \phi + \sin \theta) \quad (2.24)$$

As a measure of increase in strength, the extra stress ratio ( $\tau_{ext}/\sigma_v$ ) depends on the reinforcement force  $P_{rm}$ , the cross-sectional area of the soil on the critical plane over which a single reinforcement acts  $A_s$ , the reinforcement orientation  $\theta$ , the mobilized angle of friction  $\phi$  in the soil and the applied stress acting normally to the failure plane,  $\sigma_v$ .

6. Energy Theory. Osman (1979), developed an analytical method based on the consideration of the equilibrium of the external work due to earth pressure and the internal strain energy stored in the reinforcement ties. This method considers the behavior of a reinforced earth structure under working rather than failure conditions.

An energy relationship can be established from the elastic deformation of the wall facing and the tension in the ties due to the earth pressure. From Fig. 12, the total external work done by the earth pressure  $U_{ext}$  can be obtained from:

$$U_{ext} = B \int_0^H p(z) Y(z) dz \quad (2.25)$$

where:  $p(z)$  = the earth pressure function

$Y(z)$  = wall deflection function

$B$  = width of wall

$H$  = height of wall

Osman assumed that the external work done is stored in the ties as an elastic energy which can be calculated provided that the tie tension distribution is known. He also assumed further that:

a. A linear distribution of tension along each tie with the intensity at the wall face equal to half of the maximum intensity.

b. A parabolic deflection for the wall face as a function of the earth pressure.

c. A modulus of elasticity for the reinforced earth wall which acts as a composite material.

From the above, the maximum tension in the tie at the depth  $h$  of the fill can be calculated from:

$$T = \sqrt{\frac{6K_a^{2.5}}{L}} \gamma h \Delta H s \sqrt{H-h} \quad (2.26)$$

and the maximum tie tension in the wall is obtained from:

$$T_{max} = \sqrt{\frac{8K_a^{2.2}}{9L}} \gamma \Delta H s H^{1.5} \quad (2.27)$$

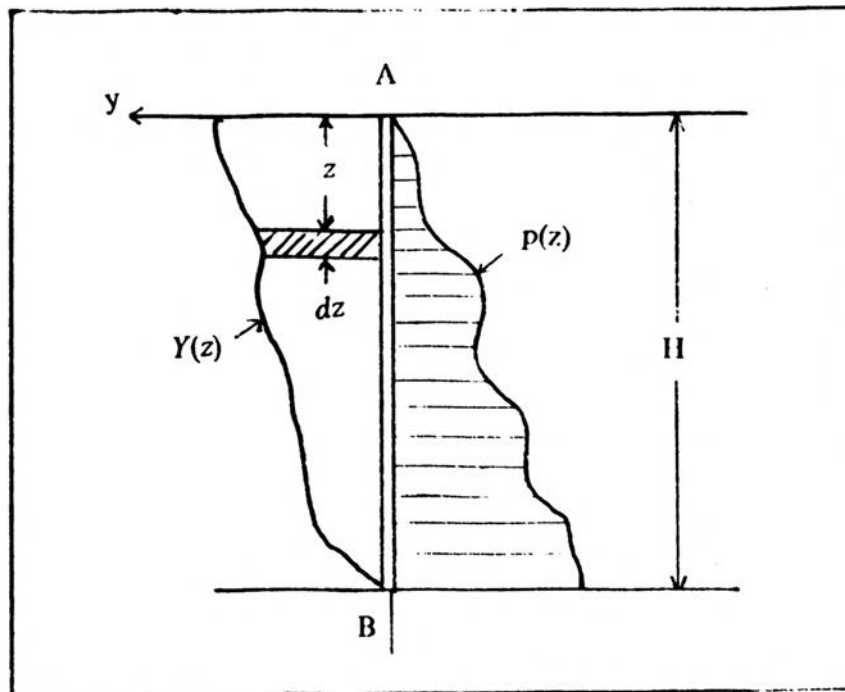


Figure 12. Energy relationship.

He also derived an expression for calculating the critical height of the wall  $H_c$ , as:

$$H_c = \left( \frac{R_t}{\gamma \Delta H s} \sqrt{\frac{9L}{8K_a^{2.5}}} \right)^{0.67} \quad (2.28)$$

Furthermore the factor of safety (F.S.) against tie pull-out can be obtained from:

$$S.F. = \frac{2bfL^{1.5}}{s\Delta H \sqrt{6K_a^{2.5}(H-h)}} \quad (2.29)$$

where:  $h$  = fill height above tie level

$\Delta H$  = vertical reinforcement spacing

$L$  = tie length

$s$  = horizontal tie spacing

$\gamma$  = unit weight of soil

$b$  = tie width

$f$  = coefficient of friction at soil-reinforcement interface

$K_a$  = coefficient of active earth pressure

$R_t$  = tensile strength of tie material

Osman carried out 35 tests on reinforced earth wall models in a rigid box 900 mm. square and 500 mm. high. Values of tie tension, strains and stresses within the soil mass were measured. The measured values of maximum tie tension are shown in Fig. 13. Also shown are the maximum theoretical tie tension envelopes derived from Rankine theory for both  $K_a$  and  $K_0$  (coefficient of earth pressure at rest) conditions, the limit state approach of Juran and Schlosser (1978) and the Energy theory. The theories, other than Rankine, indicate a distribution of tie tension which increases to a maximum and then decreases towards the base of the wall to values very much less than the Rankine values.

### C. DISCUSSION ON THEORETICAL MODELS

All of the theoretical models described so far have indicated that, in general, the strength properties of soil are improved by addition of reinforcing material.

A common assumption in the above models is that the stress distribution is uniform through each of the reinforced layers. Justification of this assumption has been questioned by several investigators who pointed out the significant effects of non-uniform stress distributions inside reinforced triaxial specimens, subjected to normal compressive stress, Chapuis (1972), and Ingold (1980).

Effects of non-uniform stress distribution on test results increase with increasing the aspect ratio of the specimen. This may well be the main reason for the observed differences between theoretical and test results. To an extent this limits one's confidence in theoretical results on one hand, and on the other hand, it may lead to erroneous conclusions in interpreting the test results. Effects of non-uniform stress distribution is decreased by reducing friction at the interfaces. This method has been used successfully for unreinforced specimens by means of lubricated end platens. However, the method cannot be applied to reinforced specimens, as the reinforcement effects are derived from mobilized friction at the soil-reinforcement interface.



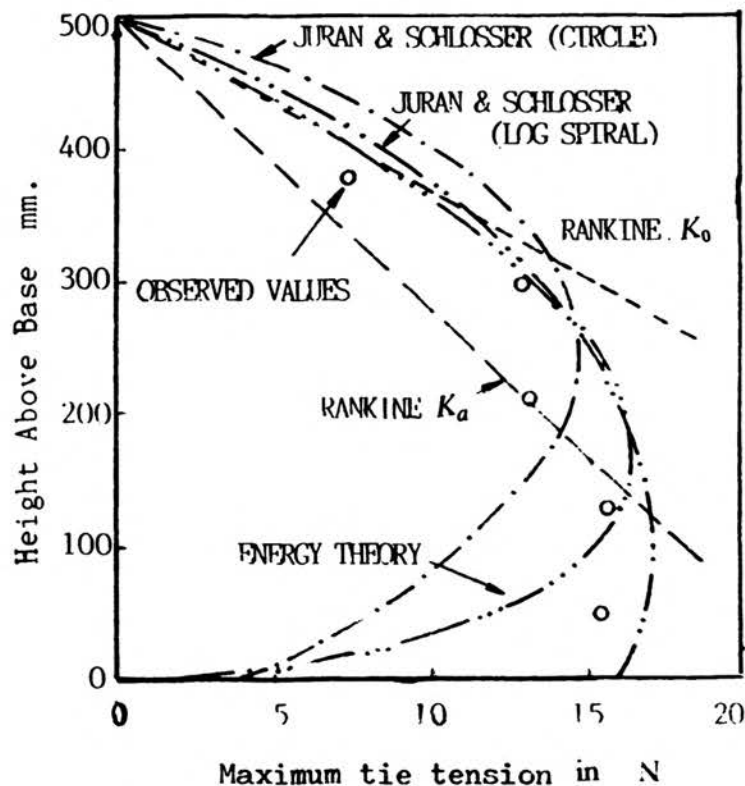


Figure 13. Observed and theoretical maximum tie tension, (after Osman, 1979).

In the following section the effects of non-uniform stress and strain distribution on shear strength of triaxial specimens are studied.

#### D. NON-UNIFORM STRESS DISTRIBUTION

In the 1860's, Tresca, while investigating the shear strength of metals, performed a number of punching tests on material confined in relatively rigid containers. He carried out one punching test on sand and observed, surprisingly, that the punch that undoubtedly had a rough base carried along an essentially undeformed cone of sand ahead of it. In 1882, Otto Mohr, criticized the commonly performed cube tests, by stating that friction acting on the end surfaces must have a great effect on the distribution of stress in the cube, so that the results could not be similar to those of a perfectly performed cubical tests in a homogeneous state of stress, (Scott, 1985).

Filon (1902), studied the problem of stress distribution inside cylinders compressed between two rough rigid platens. In his study two types of end conditions were considered:

a. A cylinder of moderate length, compressed between two rough rigid platens in such a way that the end cross sections are constrained to remain plane, and are not allowed to expand, i.e. a block of stone or masonry loaded between millboard or metal planes.

b. A cylinder constrained in such a way that the ends are allowed to expand by a definite amount, i.e. a block loaded between sheets of lead.

Based on the elastic theory, he solved these problems for the above boundary conditions and concluded that, in either case, the perimeter of the plane ends is the locus of the points where the plastic limit will first be exceeded.

Filon's analysis involved complex mathematical expressions and tedious calculations. In search of a more practical solution, this problem has been further studied by many researchers. Pickett (1944), proposed a solution for the same problem using Fourier-Bessel functions, but because of the slow convergence of the Fourier series, his results were confused near the outer edges of the specimen. D'Appolonia and Newmark (1951) developed a numerical method using a lattice analogy. Their results were similar to those of Pickett.

Balla (1960) proposed a numerical solution using a fifth degree polynomial and Fourier-Bessel functions to satisfy the boundary conditions. He introduced a new factor expressing the roughness of the loading platens. For similar boundary conditions his results were in good agreement with Filon's results. Balla further studied the effect of aspect ratio on shear strength and concluded that the compressive shear strength decreases with increasing aspect ratio. Peng (1971) used the same form of stress function as used by Balla and proposed a new solution. Later, Al-Chalabi (1973) found that the polynomial part of the stress function must be at least of the seventh order if all the boundary conditions, as well as the equilibrium conditions, are to be satisfied. Brady (1971) proposed a solution for radially end-constrained circular cylinders, but his solution contains an undetermined function. Al-Chalabi and Huang (1974) presented a closed form solution applicable to homogeneous, isotropic and elastic materials, using a ninth degree polynomial in the stress part of the function. Their solution was a function of the friction

at the interface of the specimen and end platens. Fig. 14 shows the comparison of stress distribution at the end surfaces obtained by these investigators.

Developments in computer technology in the 1960's resulted in popularity of the finite element method, which has been used by a number of researchers in solving the problem of non-uniform stress distribution within triaxial specimens. Perloff and Pombo (1969) used the finite element method to show that the significance of end effects depends upon the constitutive relations of the soil. They concluded that specimens with an aspect ratio greater than conventional should be used for those cases in which the end friction can not be reduced sufficiently. Girijavallabhan (1970) considered the problem of an axially loaded restrained cylinder, assuming linearly elastic properties. He used the finite element method and his results were similar to those of Pickett.

Dietruszczak and Mroz (1980) considered rectangular elements, rather than circular, compressed between two rigid platens and used a nonlinear finite element analysis. Their analysis was restricted to short specimens with completely rigid end platens. An interesting conclusion was that the shorter the specimen, the larger the tendency for failure initiation at the specimen corners.

Ottosen (1984) performed nonlinear axisymmetric finite element analyses on the uniaxial compression tests of concrete cylinders. His models included cylinders with aspect ratios of 1 to 3 loaded through thick steel platens. He observed that the failure mode for a cylinder having an aspect ratio of 2 consisted of two undisturbed end cones and a strain softening region in the outer portion of the middle of the cylinder. For shorter cylinders the strain softening region was more pronounced along the surface of the middle of cylinder. It is worth mentioning that Ottosen's conclusion contradicts earlier conclusions which stated that at the mid-height of the specimen, the smallest stress occurs at the outer edges.

In general, results of the finite element analyses reasonably agree with results of other numerical techniques for stress distribution at the ends. However, there is little agreement concerning stress distribution at the mid-height. This discrepancy, along with the fact that it is

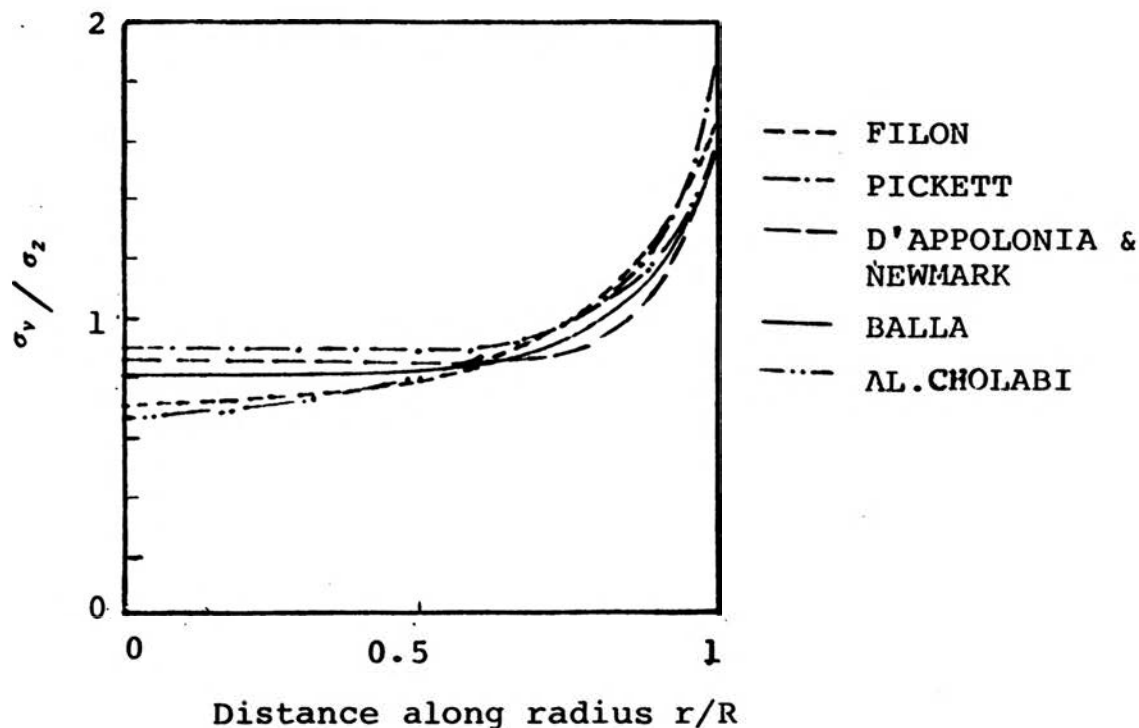


Figure 14. Comparison of stress distribution by different methods at the end surface, for perfectly confined ends.

not yet economically practical to apply the finite element method to every problem at hand has limited the wide application of this method.

Along with the theoretical investigations, laboratory experiments have been carried out by several researchers. These experiments have been performed on triaxial specimens of soil, rock, metal and concrete. Soil specimens were used more commonly as it was possible to rather easily install strain gauges, pressure cells and other measuring devices inside these specimens making them more suitable for measuring internal stress, strain and pore water pressure. On the other hand, metals have been mainly used for observing the internal deformation patterns, i.e. shear zones and rigid cones.

In an investigation performed by Mercall, Papirno, and McLaughlin (1983) on the state of stress and deformation induced in compression of metallic cylinders, relatively undeformed conical regions under the loading platens were observed, which were bordered by heavily

deformed shear zones. Close to the center of the specimen there was a region which experienced large axial strain, Fig. 15.

One of the earliest and possibly the most interesting investigation was performed by Shockley and Ahlvin (1960). Normal stress within specimens of dry sand 70in. high and 35.7in. in diameter were measured at a number of radial positions, by placing pressure cells at the mid-height of the specimen and at points just above the base. Test results showed that at mid-height, stresses in the center exceed those at the edge, whereas near the base, edge stresses were larger than those at the center. Fig. 16 shows the measured vertical stresses for 30 psi normal stress applied uniformly to the specimen. Strain measurements showed that vertical strains were small near the ends and larger toward the middle. The effects of end platens on density of fine sand specimens were also studied. These specimens were 6.5in. high and 2.8in. in diameter, with loose, medium, and dense relative density. Triaxial compression tests were also performed on dry and saturated specimens maintaining constant volume. Density measurement at different points within the specimens showed that the minimum density occurred at the center of specimens. Fig. 17 shows the density variation in a saturated sand specimen.

Bouvard and Stutz (1986) used gamma ray attenuation techniques to measure local density inside cylindrical specimens. Triaxial compression tests were performed on dry, loose and dense, coarse sand with aspect ratios of 1 and 2 using lubricated and non-lubricated end platens. In general, the test results showed that when non-lubricated end platens were used the dilation was concentrated in the middle of the specimen, Fig. 18. They also concluded that the minimum density occurs at the central part of specimen's mid-height.

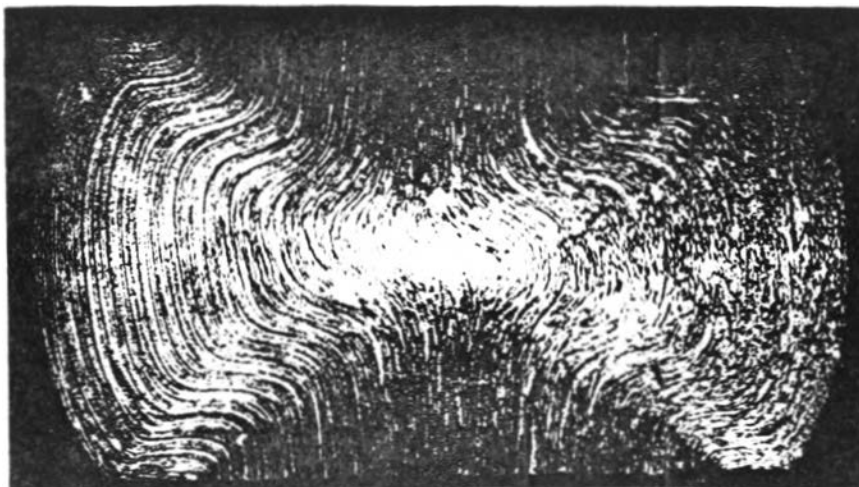


Figure 15. Section of a polished steel specimen compressed to 56% of its height, (after Mercall, Papirno and McLaughlin, 1983).

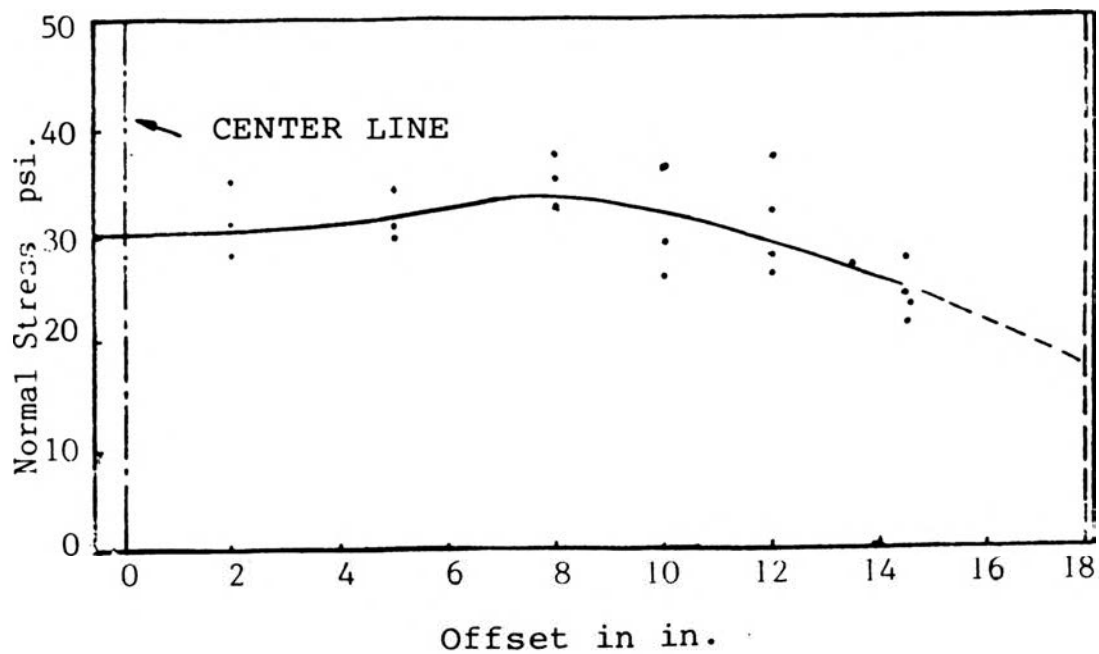


Figure 16. Variation of normal stress at mid-height, (after Shockley and Ahlvin, 1960).

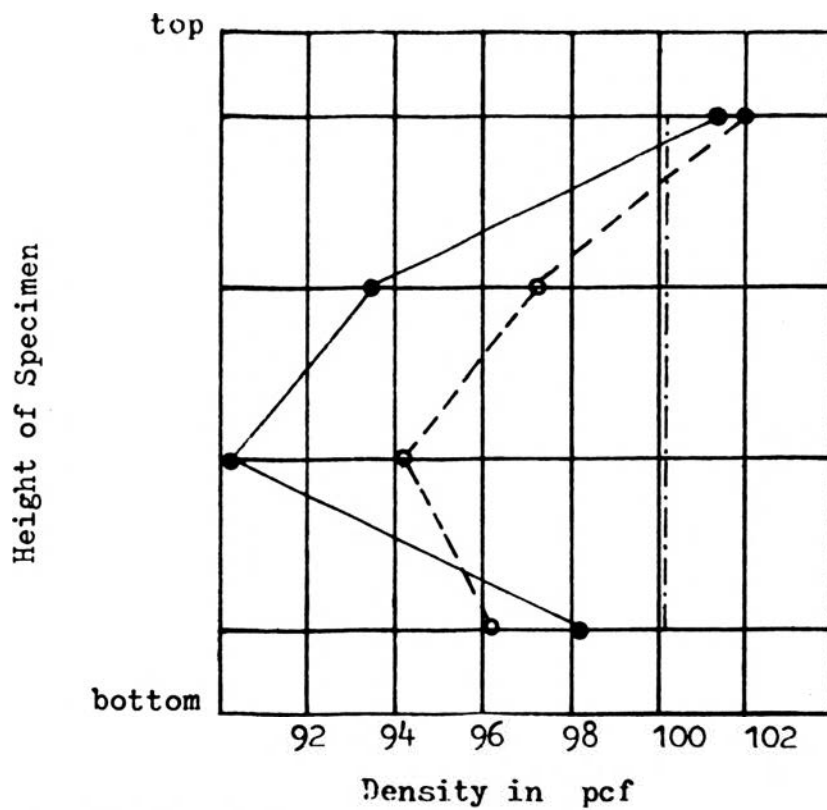


Figure 17. Density variation in saturated sand specimen, (after Shockley and Ahlvin, 1960).

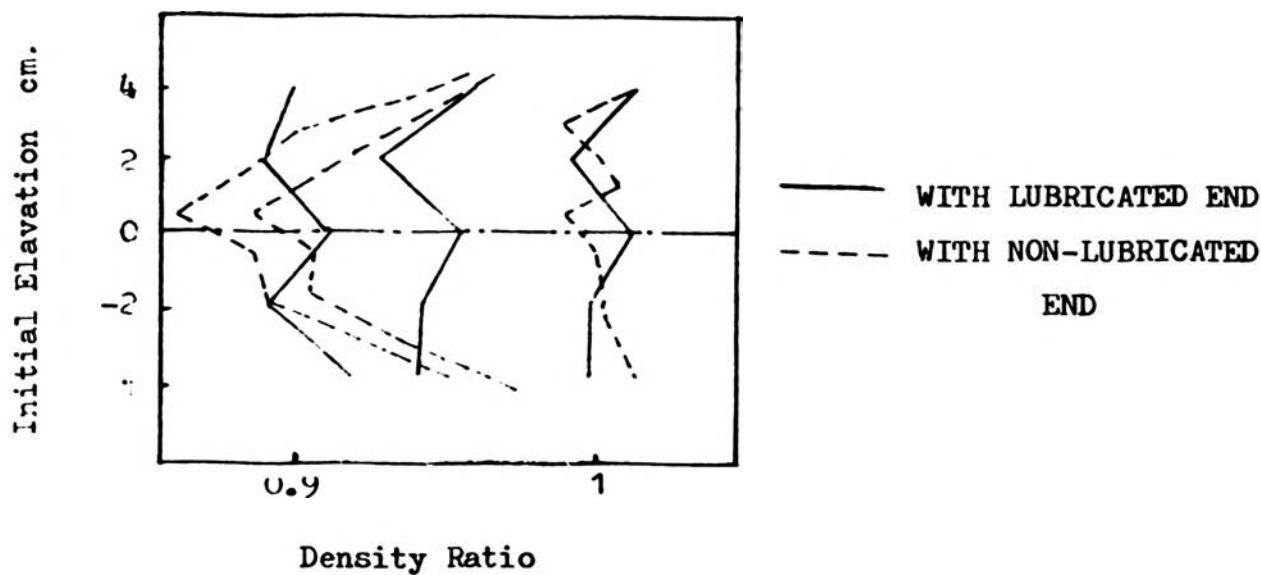


Figure 18. Density profile in triaxial specimens, (after Bouvard and Stutz, 1986).

Rowe and Barden (1964) performed a number of triaxial compression tests on sand specimens using lubricated and non-lubricated end platens and concluded that in the conventional restrained ended triaxial tests, the main dilation is confined in narrow zones as illustrated in Fig. 19. The concentration of the dilation into narrow zones causes these zones to reach the peak stress ahead of the rest of the specimen. The material in those zones thereafter becomes weaker and the stress applied to the specimen as a whole must decrease. Consequently, volume expansion must cease elsewhere in the material which has not reached its peak stress. Therefore, volume expansion is concentrated in a zone of small volume, where it progresses rapidly. A state is soon reached in which the particles have dilated so much that a group or a domain suffers a sudden collapse. However it should be noted that it is the non-uniform stress distribution which results in the concentration of stress in these small narrow zones forcing them to dilate ahead of the rest of the specimen, and not vice-versa.

Bishop and Green (1965) performed an experimental study to assess the effects of end platens on the shear strength of soils. Drained triaxial tests were carried out on saturated sand specimens 4 in. in diameter. They concluded that the end restraint increased the apparent shear strength of specimens, in an increasing rate as the aspect ratios of the specimens were increased and are of little significance when the aspect ratio is 2. Influence of the aspect ratio on the shear strength of the specimens is shown in Fig. 20.

Barden and McDermott (1965) investigated the effects of end conditions on distribution of stress and pore pressure within triaxial specimens. Undrained triaxial tests were performed on normally consolidated and overconsolidated clay specimens compacted at the dry of optimum moisture content. Change in the pore water pressure in lubricated and non-lubricated specimens were measured and are shown in Fig. 21. In this figure the solid lines indicate the change in pore water pressure at the mid-height M and at the end E of a lubricated specimen and the dotted lines show the change in pore water pressure at the same positions in a non-lubricated specimen. From the figure it is clear that pore water pressure was highly non-uniform for the non-lubricated specimen, whereas, for lubricated specimen the pore water pressure distribution was found to be uniform throughout the test. Further determination of moisture content



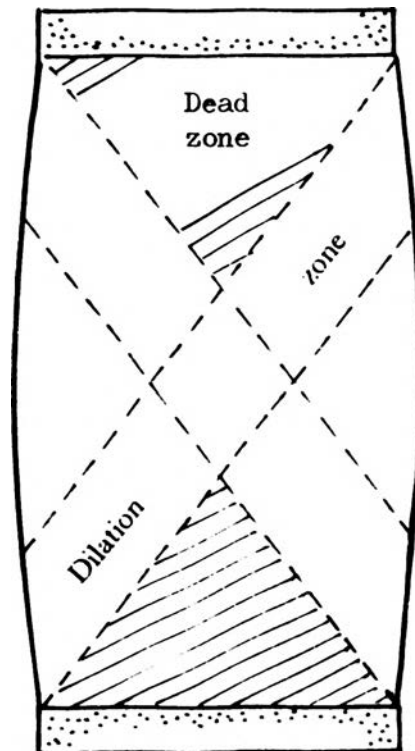


Figure 19. Dilation zone.

distribution showed that non-uniform pore water pressure resulted in non-uniform moisture content distribution inside the specimens.

Blight (1965) studied the effects of end restraint on pore water pressure distribution inside overconsolidated clay specimens ( $OCR = 16$ ), and concluded that increasing the aspect ratio is not successful in reducing the effects of end restraint. This is in contrast to the conclusion of Bishop and Green for drained tests on saturated specimens where higher aspect ratios were associated with a decrease in effects of the end restraint. Nevertheless Blight's conclusion is not surprising, since by increasing the aspect ratio, non-uniformity of stress distribution is increased and consequently variation in the pore water pressure is also increased. On the other hand, in a drained test as the aspect ratio increases, the adverse effects of non-uniform stress distribution reduces the restraining effect of the end platens and cause the specimen to fail under a lower external stress.

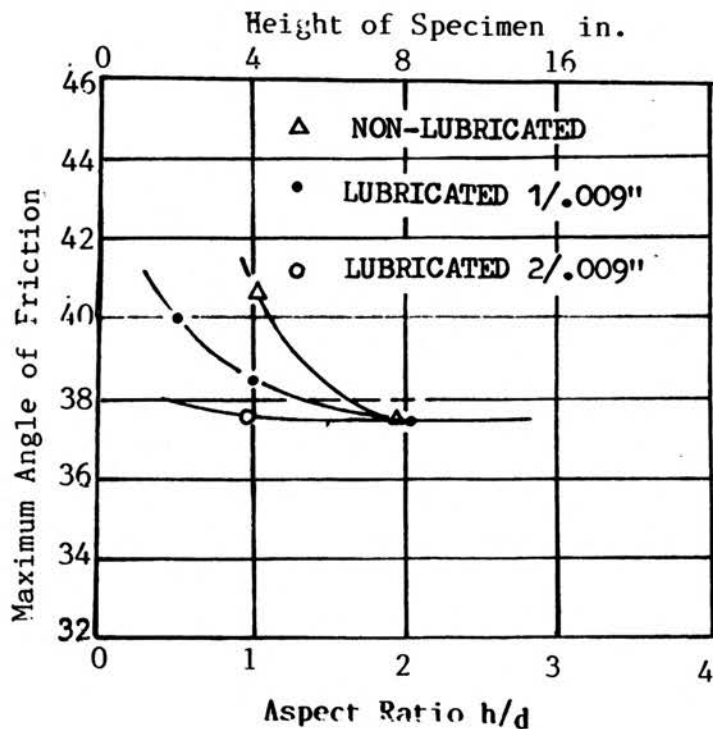


Figure 20. Influence of aspect ratio on shear strength of specimens with various degrees of end restraint, (after Bishop and Green, 1965).

Kirkpatrick and Belshaw (1968) used an X-ray technique in measuring internal displacements of medium dense sand specimens. They concluded that non-uniform strains were due to the formation of quasi-rigid zones near the rough end platens. Kirkpatrick and Younger (1970) used the same technique and concluded that the use of rough platens results in the development of highly non-uniform strain, which increases as the aspect ratio of the specimen is decreased. Distributions of axial strain at distances  $h/2$  and  $h/8$  from the end, across the width of a sand specimen loaded through rough platens are shown in Fig. 22. Further, the formation of dead zones at the specimen's ends is caused by the restraining effect of radial friction force at the end platens. Fig. 23 shows the shape of the end zones which were formed close to the rough platens.

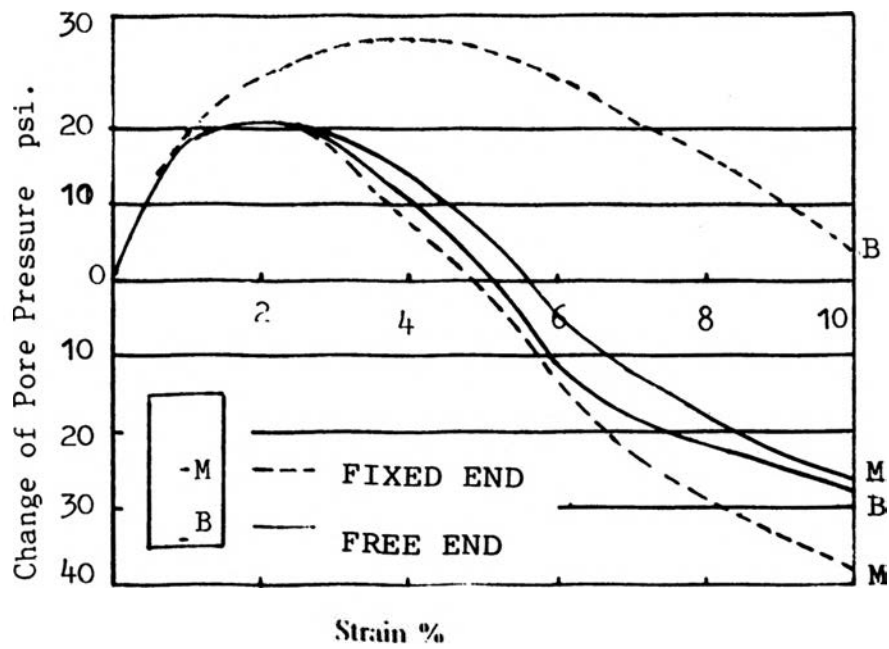


Figure 21. Pore pressure distribution at the end and mid-height of specimens with fixed ends and free ends, (after Barden and McDermott, 1965).

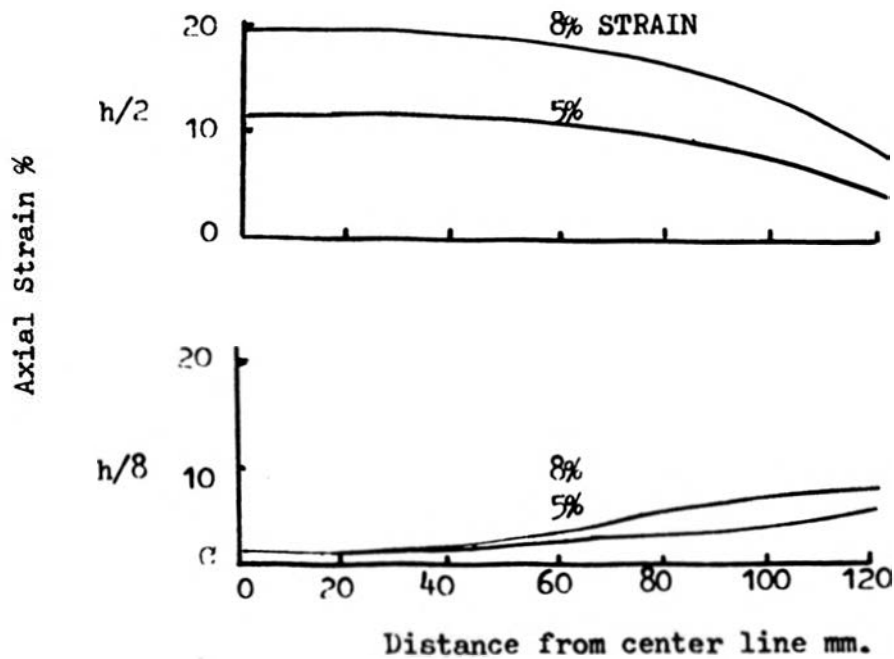


Figure 22. Distribution of axial strain in specimen with rough ends at  $h/2$  and  $h/8$ , (after Kirkpatrick and Younger)

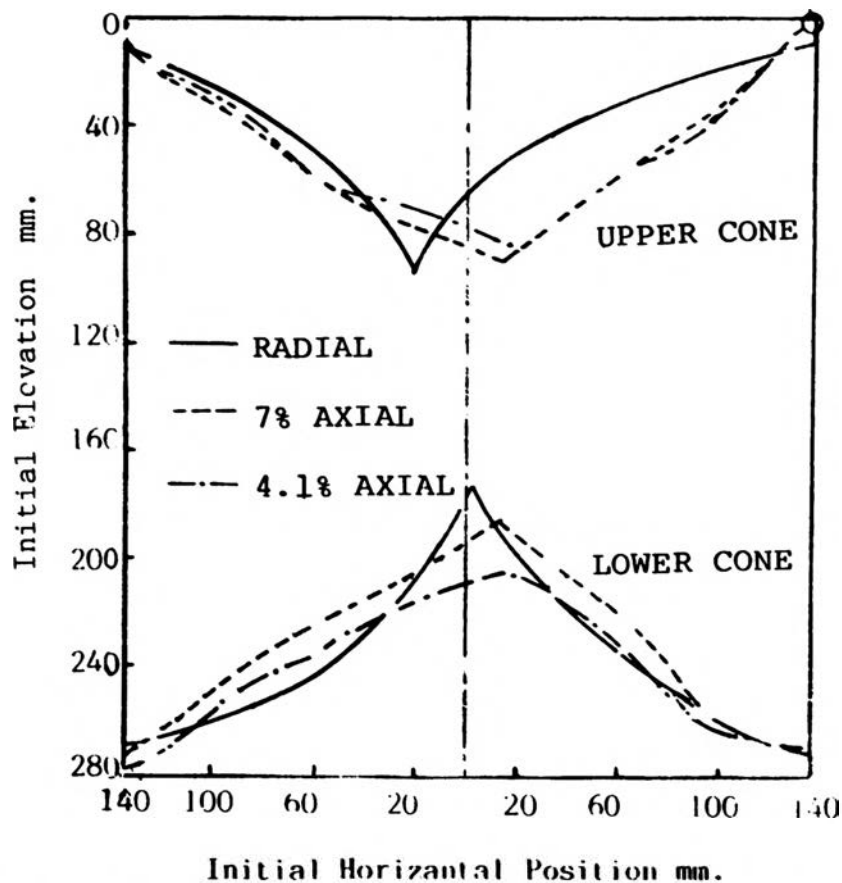


Figure 23. Rigid end zones in triaxial specimen loaded through rough end platens, (alter Kirkpatrick and Younger, 1970)

#### E. DISCUSSION ON NON-UNIFORM STRESS AND STRAIN DISTRIBUTION

The problem of non-uniform stress and strain distribution within triaxial specimens has been studied both analytically and experimentally by many researchers for over a century. Several approximate solutions using mathematical and finite element techniques have been proposed for computing non-uniform stress distribution under several boundary conditions. In the experimental work the effects of non-uniform state of stress and strain within the specimens have been reduced either by lubricating the end platens, or by choosing an appropriate aspect ratio.

On the other hand, analytical and experimental models have not been used extensively due to one or more of the following reasons:

a. In general the proposed analytical methods are tedious and time consuming and are not practical.

b. Use of lubricated ends has proved to be an effective way of reducing end restraint and hence, non-uniform stress and strain distributions. This method is extensively used in research and experimental investigations, but it is not as widely used in every day practice.

c. By using an appropriate aspect ratio. However, in practice regardless of the type of soil and/or end platens, an aspect ratio of 2 is usually used.

Since the above described methods are not feasible in assessing the true stresses acting within reinforced triaxial specimens, it would be beneficial to develop a simple analytical model which can be used in assessing the values of stress at various points within the specimens.

### III. PROPOSED MODELS

Two analytical models are developed. In the first model, effects of end friction on shear strength of triaxial specimens are considered. The second model considers the problem of non-uniform stress distribution and can be used in calculating the magnitude of normal stress at any point within triaxial specimens.

#### A. ENHANCED CONFINING PRESSURE MODEL

1. Uniform Stress Distribution in Triaxial Specimens. In a triaxial specimen subjected to normal stresses at its boundaries (Fig. 24.a & b) the state of stress and strain are homogeneous if frictional force is not developed at the end surfaces. That is, at any point within the specimen, (Fig. 24.b):

$$\sigma_2 = \sigma_1$$

$$\sigma_r = \sigma_\theta = \sigma_3 \quad (3.1)$$

$$\tau_{rz} = \tau_{z\theta} = \tau_{r\theta} = 0$$

where:  $\sigma_z$  = normal stress at any point within the specimen.

By assuming that the Mohr-Columb's envelope is valid at failure we can write:

$$\sigma_1 = K_p \sigma_3 \quad (3.2)$$

In practice most of the triaxial specimens are loaded through rough surfaces and friction at the end surfaces is large, e. g., the angle of friction developed between sand and smooth pyrex glass is at least 5 degrees, (Totsuoka and Haibava, 1985). Hence, by applying a compressive stress  $\sigma_1$ , (Fig. 25.a & b) to the specimen, a frictional stress  $\tau$  is mobilized at the interfaces. The induced frictional stress restrains lateral expansion of the specimen and leads to a non-uniform state of stress and strain, (Shockley and Ahlvin, 1960). The problem of non-uniform state of

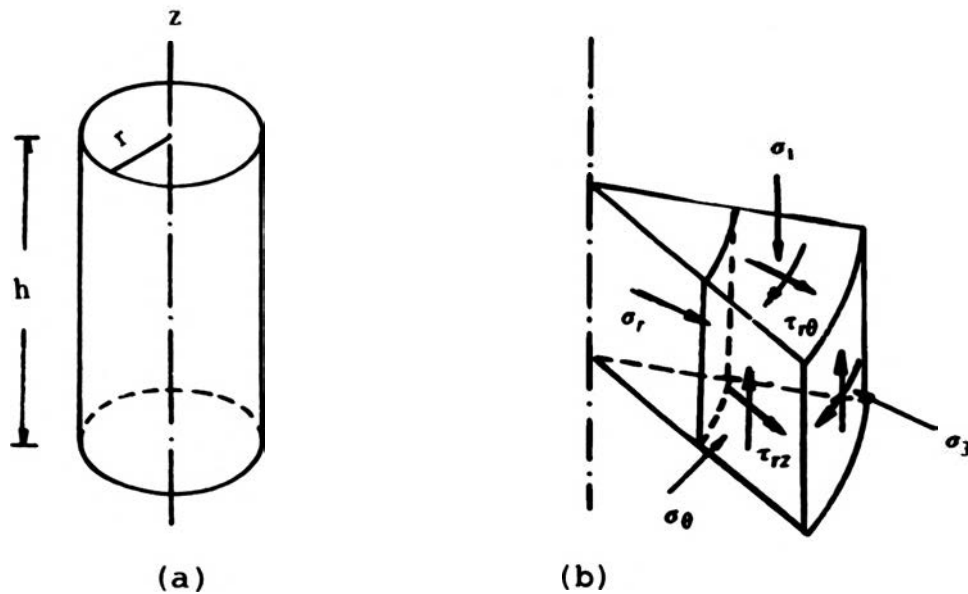


Figure 24. Homogeneous state of stress in triaxial specimen.

stress and strain is even more pronounced in reinforced soil specimens as the angle of friction at the soil-reinforcement is usually much larger.

2. **The Model.** Stresses acting on a triaxial specimen loaded through rough surfaces are schematically shown in Fig. 25. A frictional stress  $\tau$  is mobilized at the interfaces which affects the magnitude of failure normal stress  $\sigma_{1r}$ , which can be calculated from  $\sigma_{1r} = \sigma_1 + \Delta\sigma_1$ , in which  $\sigma_1$  is the failure stress for the same specimen when loaded through lubricated surfaces. If it is considered that the Mohr-Coulomb envelope is valid at failure then we can write:

$$\sigma_{1r} = K_p \sigma_{3r} \quad (3.3)$$

in which  $\sigma_{3r} = \sigma_3 + \Delta\sigma_3$ . By using 3.3 and substituting the values of  $\sigma_{1r}$  and  $\sigma_{3r}$  we get:

$$\begin{aligned} \sigma_1 + \Delta\sigma_1 &= K_p(\sigma_3 + \Delta\sigma_3) \\ \Delta\sigma_1 &= K_p \Delta\sigma_3 \end{aligned} \quad (3.4)$$

Now consider the radial equilibrium of a disc of material of radius  $r$  and height  $h$  being compressed between rough platens and assume that:

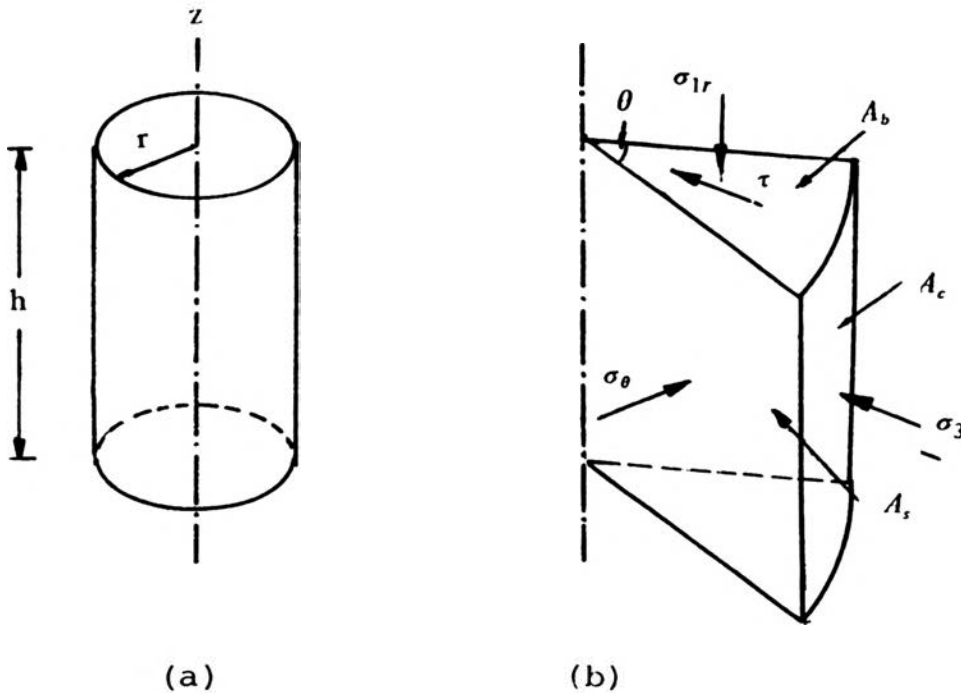


Figure 25. Stress acting on a triaxial specimen loaded through rough surfaces.

- a. The applied normal stress  $\sigma_{1r}$  at failure is an effective stress.
- b. Height of specimen  $h$  is small and, hence, stress distribution is uniform within the specimen.
- c. Radial and circumferential stress components  $\sigma_r$  and  $\sigma_\theta$  (Fig. 24.b) are equal and both are principal stresses.
- d. The magnitude of the mobilized frictional stress  $\tau$  at failure is proportional to the applied normal stress at failure and is equal to:

$$\tau = \sigma_{1r} \tan \delta \quad (3.5)$$

where:  $\delta =$  angle of bond stress at the interface

Hence we can write, (Fig. 25.b):

$$\sigma_z = \sigma_{1r}$$

$$\sigma_r = \sigma_\theta = \sigma_3 + \Delta\sigma_3 \quad (3.6)$$



Summation of forces in the radial direction (Fig. 25.b) leads to:

$$2 \tau A_b + \sigma_3 A_c = 2 \sigma_\theta A_s \left( \sin \frac{\theta}{2} \right) \quad (3.7)$$

where:  $A_b$  = cross sectional area of section =  $r^2 \theta/2$

$A_c$  = surface area of section =  $(r \theta) h$

$A_s$  = surface area of one side of section =  $r h$

Further, for small values of  $\theta$ ,  $\sin \theta/2$  can be replaced by  $\theta/2$ . Substituting the values of  $A_b$ ,  $A_c$  and  $A_s$  from the above and  $\sigma_\theta$  from 3.6 into 3.7 we have:

$$2 \tau \left( \frac{r^2 \theta}{2} \right) + \sigma_3 (r \theta) h = 2(\sigma_3 + \Delta \sigma_3) r h \left( \frac{\theta}{2} \right) \quad (3.8)$$

From which we get:

$$\tau r = h \Delta \sigma_3 \quad (3.9)$$

By substituting the value of  $\tau$  from 3.5 into 3.9 and rearranging the terms, the value of enhanced confining pressure can be calculated from:

$$\Delta \sigma_3 = \frac{r}{h} \sigma_{1r} \tan \delta \quad (3.10)$$

Furthermore change in the failure normal stress  $\Delta \sigma_1$  for both unreinforced and reinforced specimens can be calculated from 3.4 and 3.10, as:

$$\Delta \sigma_1 = \frac{K_p}{2\eta} \sigma_{1r} \tan \delta \quad (3.11)$$

where:  $\eta = \frac{h}{d}$

By substituting the value of  $\Delta \sigma_1 = \sigma_{1r} - \sigma_1$  into 3.11 and solving for  $\sigma_{1r}$ , we can calculate the magnitude of failure normal stress from:

$$\sigma_{1r} = \frac{2 \eta \sigma_1}{2 \eta - K_p \tan \delta} \quad (3.12)$$

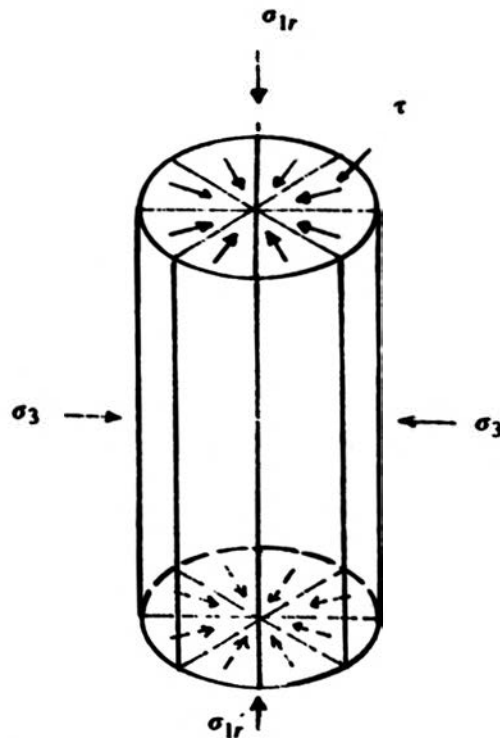


Figure 26. Cylindrical specimen composed of  $n$  sections.

### B. BEAM-COLUMN MODEL

When the aspect ratio of the specimen is increased, non-uniformity of stress and strain, and hence, the strength properties of the specimen is affected. In order to estimate the magnitude of normal stress at any point within the specimen let us assume that the specimen is composed of  $n$  imaginary sections, Fig. 26. By inspection it is clearly seen that stresses acting on each section (Fig. 27.a) can be shown to be the sum of state of stress in Fig's 27.b and 27.c. However, the stresses in Fig. 27.b are the same as the stresses acting on a section of specimen loaded through lubricated surfaces, and hence, are associated with a uniform state of stress. On the other hand, stresses in Fig. 27.c are only present in the specimens loaded through rough surfaces. Therefore, it can concluded that they are the primarily cause of non-uniform state of stress.

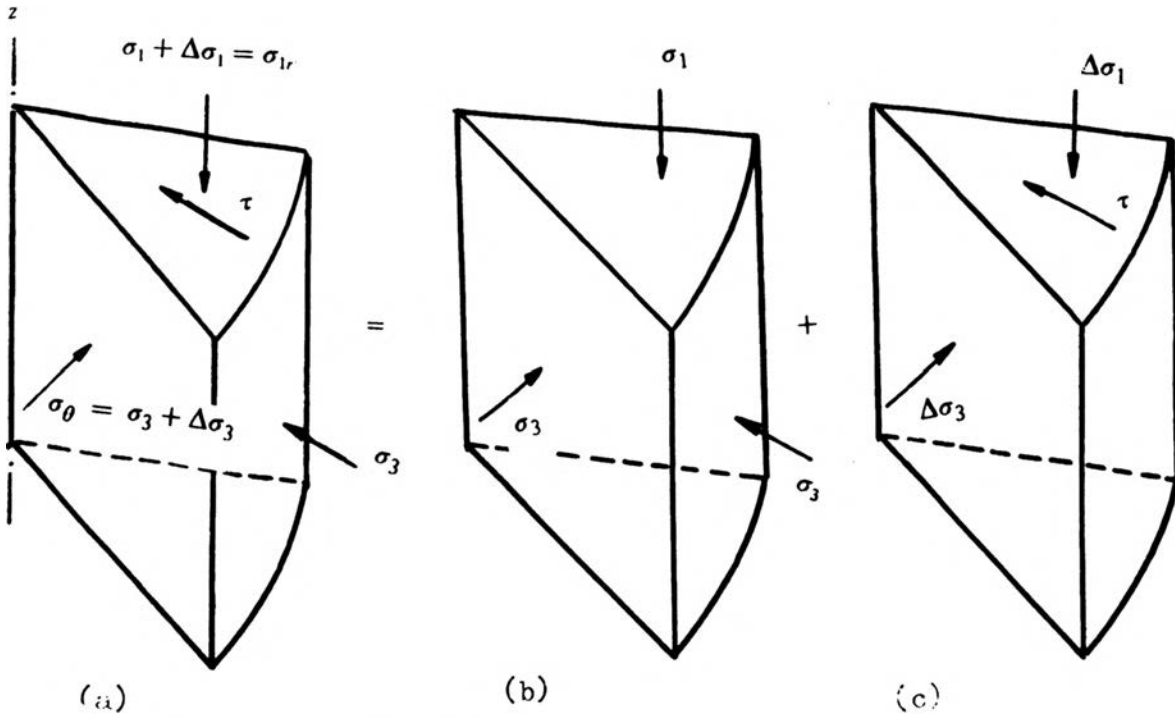


Figure 27. Stress acting at each section of specimen.

Further inspection of Fig. 27.c shows that it can be considered as a beam-column member. By considering the free body diagram of Fig. 27.c separated by plane m-m, as shown in Fig. 28. The magnitude of normal stress acting at any point inside the section can be calculated from:

$$\Delta\sigma_2 = \Delta\sigma_1 \pm \frac{MC}{I_r} \quad (3.13)$$

where:  $M$  = bending moment about horizontal axis.

$C$  = distance from centroid.

$I_r$  = moment of inertia of the section about radial axis.

For a small  $\theta$  the cross section of the beam-column element (Fig. 27.c) can be approximated by a triangle and hence the magnitude of normal stress  $\sigma_z$  at any point within the specimen can be calculated from:

$$\sigma_z = \sigma_1 + \Delta\sigma_1 \pm 36 \frac{MC}{\theta r^4} \quad (3.14)$$

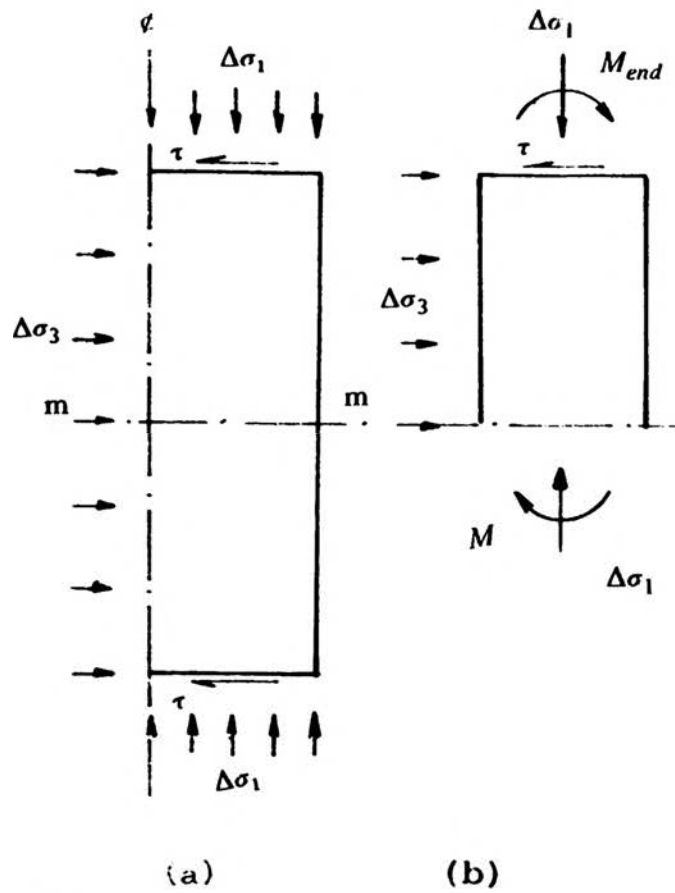


Figure 28. Free-body diagram

The magnitude of bending moment  $M$  depends on the boundary condition (end moment) at the interfaces and has a general form of  $k(\Delta\sigma_3 h^2)$ , where the value of  $k$  depends on the boundary condition. Therefore we can write:

$$\sigma_z = \sigma_1 + \Delta\sigma_1 \pm 36k \frac{\Delta\sigma_3 h^2 C}{r^4 \theta} \quad (3.15)$$

Substituting the value of  $\Delta\sigma_3$  from equation 3.10 and knowing that  $\sigma_1 + \Delta\sigma_1 = \sigma_{1r}$ , results in an expression for calculating the value of normal stress at any point within the specimen:

$$\sigma_z = \sigma_{1r} \left( 1 \pm k' \frac{\eta \tan \delta C}{r^2 \theta} \right) \quad (3.16)$$

Where:  $k' = 72k$

Equation 3.16 can be used for calculating the magnitude of normal stress within triaxial specimens provided that:

- a. Boundary conditions at interfaces are known.
- b. Aspect ratio ( $h/r$ ) of the specimen is large.
- d. Frictional stress at interfaces is proportional to the applied normal stress.

### C. STATE OF STRESS AT FAILURE

The proposed Beam-Column model can be used to examine the state of stress at any point within triaxial specimens. At the mid-height, bending stress is compressive at the center and hence, normal stress  $\sigma_z$  is larger than the applied normal stress  $\sigma_{1r}$ . Also the bending stress is tensile at the edges and hence, normal stress  $\sigma_z$  is smaller than the applied normal stress. On the other hand, for the ends, bending stress is tensile at the center and compressive at the edges. Fig. 29 schematically shows the normal stress distribution at the end and mid-height of a triaxial specimen based on the above reasoning. It shows that at mid-height of the specimen, maximum normal stress occurs at the center, and minimum normal stress occurs at the edges. On the other hand, at the ends of the specimen, normal stress is maximum at the outer edges and minimum at the center. Mohr-Coulomb's failure envelope for points A and B at mid-height of the specimen is shown in Fig. 30 and the failure envelope for points C and D is shown in Fig. 31.

### D. EFFECTS OF ASPECT RATIO ON STRENGTH

Effect of end friction on shear strength of triaxial specimens is a rather complex phenomenon. On one hand, the enhanced confining pressure increases the strength of the specimen. On the other hand, it affects the distribution of normal stress within the specimen and results in a normal stress which is larger in magnitude than the applied normal stress at the center of the specimen. Furthermore, by assuming that the mobilized friction at the ends of the specimen is not a function of the height of the specimen, the magnitude of enhanced confining pressure  $\Delta\sigma_3$  decreases as the height of specimen increases (the same force is distributed on a larger surface area). At the same time, increase in the height is accompanied by increase in the

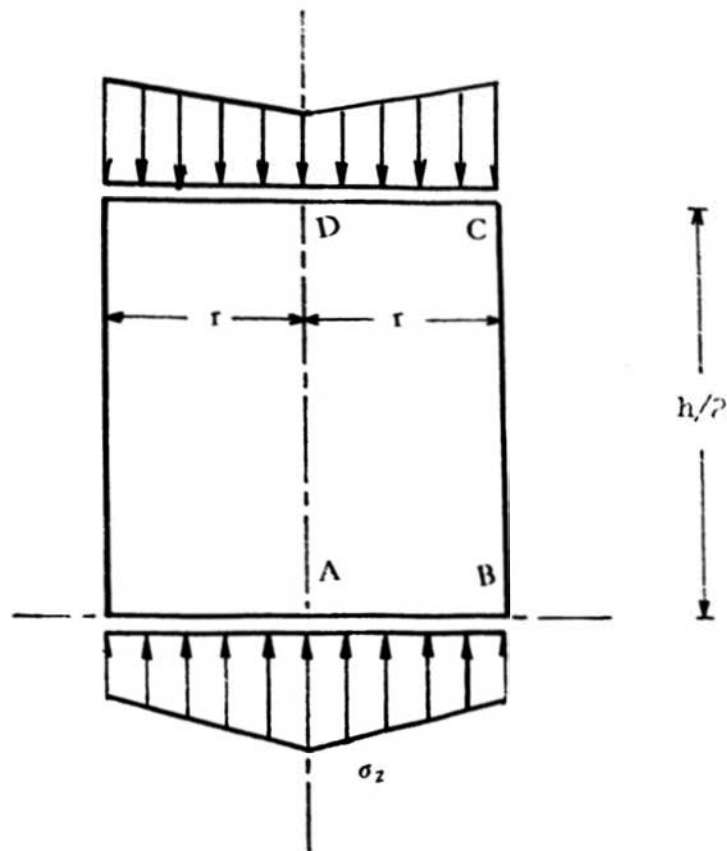


Figure 29. Normal stress distribution at the end and mid-height of a triaxial specimen loaded through rough surfaces.

mobilized bending stress within the specimen which causes a further increase of the normal stress at the center of the specimen.

Therefore it can be concluded that for a soil specimen loaded through non-lubricated surfaces, the increase in the enhanced confining pressure caused by the end friction is counteracted by the increase in the normal stress at the center of the specimen due to the induced bending stress. For a specimen with a small aspect ratio, the effect of the end friction is greater and the specimen fails at a higher normal stress. For a specimen with a large aspect ratio the effects of the increase in the normal stress is larger and the specimen fails at a lower normal stress.

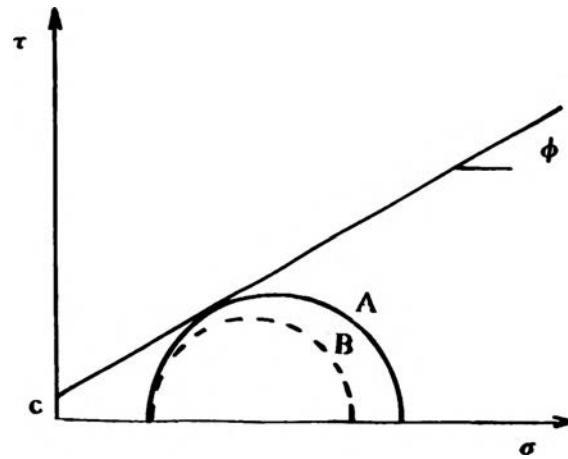


Figure 30. Mohr-Coulomb failure envelope for points A and B.

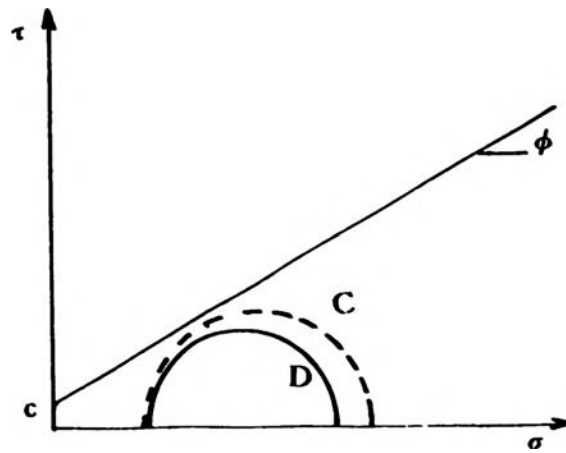


Figure 31. Mohr-Coulomb failure envelope for points C and D.

#### IV. TESTS RESULTS AND DISCUSSION

Laboratory triaxial tests were performed on a loessial soil obtained from a borrow site located near Collinsville, in the south of Madison county Illinois, approximately 12 miles to the east of St. Louis. In the laboratory, the soil was air dried and then thoroughly remolded using a mechanical grinder. Results of the preliminary investigation showed that the loess may be classified as ML. Index properties of the loess were determined and are listed in Table I. Standard Proctor compaction tests were performed and the dry density versus water content relationship of the loess was established and is shown in Fig. 32. Triaxial compression tests were performed on unreinforced and reinforced loess specimens compacted to 95 percent of maximum dry density and moisture content of 12 and 17 percent.

##### A. PROCEDURES AND TEST DATA

1. Reinforcing Material. Today most engineering fabrics or geotextiles in widespread use are made from polymeric materials or fibers. Typical polymers are polypropylene, polyester, polyethylene, and polyamide. The two most common types of geotextiles are woven and non-woven fabrics. The former is manufactured from two sets of parallel filaments or yarn oriented in two mutually perpendicular directions. Non-woven fabric consists of a mat of fibers of either continuous or discrete length filaments, arranged in a random pattern and bonded together mechanically, thermally, or chemically.

A satisfactory soil-reinforcement system must exhibit several attributes not least of which is the ability to generate high soil reinforcement bond. This quality is particularly vital in low strength cohesive fills where the soil itself is potentially the weak link in the soil-reinforcement chain. However, reinforcing bond can be reduced drastically by build up of pore pressure which can cause adverse effects on shear strength. Triaxial compression tests on saturated clay specimens showed that shear strength of clay was reduced by as much as 40 percent when the specimens were reinforced with non-permeable (aluminum foil) material, Ingold (1980).



Table I. INDEX PROPERTIES OF LOESS

|                       |       |     |
|-----------------------|-------|-----|
| Specific Gravity      | 2.69  |     |
| Liquid Limit          | 28.6  | %   |
| Plastic Limit         | 22.4  | %   |
| Plasticity Index      | 6.2   | %   |
| Optimum water content | 14.2  | %   |
| Maximum Dry Density   | 110.8 | pcf |

A preliminary investigation was carried on in order to select a suitable reinforcing material. Properties of several available geotextile fabrics were compared and a commercial woven geotextile from Exxon chemicals was chosen. Table II shows properties of the geotextile fabric (furnished by the manufacturer).

2. Compaction. Specimens are compacted by kneading compaction, by a method similar to the Harvard Miniature compaction, but with larger resultant specimens. A special split compaction mold is used to prepare the specimens. The mold consists of an outer tube of steel pipe with an inside thin walled steel tube 2.83 in. (72 mm.) in diameter. The mold is such that when the machine bolts on the outer casing are loosened, the split steel tube inside the mold expands and allows for removal of the specimen with minimum effort and disturbance.

A preliminary compaction investigation was undertaken in an attempt to relate the number of tamps to dry density of the soil. The number of tamps were determined for each moisture content at the desired density. In order to minimize moisture content variation the loess was brought to designated moisture content (12 and 17 percent) in large batches and sealed in air tight bags and placed in a moist curing room for a minimum of three days.

Table II. PROPERTIES OF GEOTEXTILE FABRIC GTF-200.

|                                  |                        |      |        |
|----------------------------------|------------------------|------|--------|
| Wide Width Strut Tensile         | ASTM D-4532            | 270  | psi    |
| Grab Tensile Strength            | ASTM D-1682            | 200  | lb     |
| Secant Modulus at 10% Elongation | ASTM D-1682            | 670  | lb/in  |
| Elongation                       | ASTM D-1682            | 20   | %      |
| Permeability Coefficient         | Falling Head 40cm-10cm | 0.02 | cm-sec |

3. Specimen Preparation. The compaction mold was assembled, and its inside was sprayed lightly with a silicone compound to reduce the possibility of sticking the specimen to its side. A sheet of Mylar film was placed around the inside of the mold to facilitate specimen removal. The wet weight of the specimen at the desired density (95 percent of maximum dry density) was determined, and the weight of each layer of soil was calculated. A batch of soil was placed in the mold, leveled off and carefully compacted by a tamper similar to a Harvard Miniature compaction tamper, modified by a longer piston and a 1.125in. (28.6mm.) diameter circular foot and a spring pressure of 44 pounds was used. Uniformity of the specimens were further controlled by carefully monitoring the thickness of each layer. After tamping the upper portion of the soil layer was scarified with a spatula, and another batch of soil was placed in the mold, leveled off, and compacted. This procedure was repeated until the top of the soil specimen was one layer above the main body of the mold. The compaction collar was then removed and the soil was trimmed flush with the top of the mold. The weight of the specimen was determined. The specimen was wrapped in plastic sheet, put into two zippered bags, labeled and placed in the humid room for three days of another "curing".

The same procedure was followed in preparing the reinforced specimens except that at the desired heights, a 2.83 in.(72 mm.) diameter disc of the reinforcing fabric was placed on top of the compacted layer, and then the next batch of the soil was placed in the mold.

4. Triaxial Testing. A total of 22 unconsolidated undrained triaxial compression tests were conducted in two phases. In the first phase, 6 unreinforced loess specimens were tested. In the second phase, 16 reinforced specimens with 5 different aspect ratios were tested.

5. Phase-one Unreinforced Specimens. In order to assess the effect of reinforcement on strength properties of the soil, it is first necessary to define the strength properties of the unreinforced soil. Hence, phase one of the testing program was performed on six unreinforced loess specimens 2.83 in. (72 mm.) in diameter and 5.67 in. (144 mm.) in height. The specimens were prepared at a predefined degree of compaction (95 percent of maximum dry density) at two different moisture contents (12 and 17 percent), and were subjected to confining pressures of 10, 20, or 30 psi. (69, 138 and 207 kPa.) respectively.

To insure a uniform state of stress and strain within the specimens, end platens were lubricated in this phase of the testing program. At first a thin layer of silicone vacuum grease was applied to each end-platen, and a thin rubber membrane disc was cut and placed over the grease on each platen. The specimen was placed on the base platen, the top platen was put on its top, and then a rubber membrane was placed around it.

The triaxial cell was assembled and filled with deaired water. The desired confining pressure was applied, and the specimen was sheared at a constant strain rate of 2 percent per minute. Axial loads were read through a calibrated load cell at predetermined axial deformation until failure or 20 percent strain, whichever occurred first. Then the specimen was removed from the triaxial cell, weighed, and the entire specimen was placed in the oven for moisture content determination. Results of this phase of testing program (tests No. 1-6) are given in Table III.

6. Phase-Two Reinforced Specimens. In the second phase of the testing program, reinforced specimens were tested with the same moisture contents and compaction effort as in the phase-one of the testing program. In this phase, the same procedures as those employed in the first phase of the testing program were used, except that in place of rubber membrane a disc of reinforcing fabric was placed on each end platen.

At a moisture content of 12 percent, 3 reinforced specimens with an aspect ratio of 0.4 were tested (tests No. 7-9). At 17 percent moisture content, 13 reinforced specimens with aspect ratios of 0.4, 0.5, 0.67, 1, and 2 were tested (Tests No. 10-22). Test results are given in Table IV.

## B. TEST DATA

Plots of deviator stress versus longitudinal strain for unreinforced specimens (tests No. 1-6) are shown in Fig. 33.

Results of tests No. 7-9 are plotted in Fig. 34. These specimens were prepared at 12 percent moisture content and reinforced with six reinforcing discs, one on each end platen and 4 spaced equally at 1.13 in. (29 mm.) center to center.

Fig. 35 shows the results for tests No. 10-12. These tests were performed on reinforced specimens prepared at 17 percent moisture content and an aspect ratio of 0.4 (with the same reinforcement arrangement as tests No. 7-9).

Tests results for No. 13-15 are plotted in Fig. 36. These tests were performed on reinforced specimens prepared at 17 percent moisture content with an aspect ratio of 0.5. In these specimens five reinforcing discs were used at 1.41 in. (35 mm.) center to center.

Fig. 37 shows the results of tests No. 16-18 on reinforced specimens with aspect ratio of 0.67. Four reinforcing discs were used at 1.83 in. (46 mm.) center to center.

In order to confirm the repeatability of the test results, three pairs of identical tests were performed on reinforced specimens with 17 percent moisture content, and aspect ratios of 0.5, 1.0, and 2.0, subjected to 30psi. (207kPa.) confining pressure. Test results are given in Fig. 38, which shows that the tests were indeed highly reproducible.

Table III. TRIAXIAL TEST RESULTS (UNREINFORCED SPECIMENS)

| Test No. | Confining Pressure<br>psi. | Moisture Content<br>% | Deviator Stress<br>psi. | Aspect<br>Ratio |
|----------|----------------------------|-----------------------|-------------------------|-----------------|
| 1        | 10                         | 12.2                  | 47.45                   | 2               |
| 2        | 20                         | 12.4                  | 65.35                   | 2               |
| 3        | 30                         | 12.4                  | 82.10                   | 2               |
| 4        | 10                         | 17.0                  | 34.07                   | 2               |
| 5        | 20                         | 17.2                  | 55.41                   | 2               |
| 6        | 30                         | 17.4                  | 77.57                   | 2               |

Table IV. TRIAXIAL TEST RESULTS (REINFORCED SPECIMENS)

| Test No. | Disc Spacing<br>in. | Confining<br>Pressure psi | Moisture<br>Content % | Deviator<br>Stress psi | Strength<br>Ratio | Aspect<br>Ratio |
|----------|---------------------|---------------------------|-----------------------|------------------------|-------------------|-----------------|
| 7        | 1.134               | 10                        | 12.2                  | 117.12                 | 2.47              | 0.40            |
| 8        | 1.134               | 20                        | 12.2                  | 192.02                 | 2.97              | 0.40            |
| 9        | 1.134               | 30                        | 11.8                  | 228.69                 | 2.78              | 0.40            |
| 10       | 1.13                | 10                        | 17.2                  | 100.43                 | 2.95              | 0.40            |
| 11       | 1.13                | 20                        | 17.0                  | 161.09                 | 2.91              | 0.40            |
| 12       | 1.13                | 30                        | 16.9                  | 215.05                 | 2.77              | 0.40            |
| 13       | 1.41                | 10                        | 17.0                  | 94.69                  | 2.77              | 0.50            |
| 14       | 1.41                | 20                        | 17.0                  | 122.69                 | 2.21              | 0.50            |
| 15       | 1.41                | 30                        | 17.2                  | 154.19                 | 1.99              | 0.50            |
| 16       | 1.83                | 10                        | 17.1                  | 48.94                  | 1.43              | 0.67            |
| 17       | 1.83                | 20                        | 17.0                  | 71.06                  | 1.28              | 0.67            |
| 18       | 1.83                | 30                        | 17.1                  | 126.10                 | 1.62              | 0.67            |

Table IV. TRIAXIAL TEST RESULTS (REINFORCED SPECIMENS) CONTINUED.

| Test No. | Disc Spacing<br>in. | Confining<br>Pressure psi | Moisture<br>Content % | Deviator<br>Stress psi | Strength<br>Ratio | Aspect<br>Ratio |
|----------|---------------------|---------------------------|-----------------------|------------------------|-------------------|-----------------|
| 19       | 2.83                | 30                        | 17.3                  | 95.71                  | 1.23              | 1.00            |
| 20       | 2.83                | 30                        | 17.1                  | 91.94                  | 1.18              | 1.00            |
| 21       | 5.67                | 30                        | 17.2                  | 72.54                  | 0.93              | 2.00            |
| 22       | 5.67                | 30                        | 17.5                  | 74.53                  | 0.96              | 2.00            |

### C. ANALYSIS OF TESTS RESULTS

Test results for reinforced specimens (tests No. 7-22) have been given in Table IV. In this table deviator stresses are listed in column 5, and strength ratios are listed in column 6. The strength ratio is defined as the ratio of the measured deviator stress at failure of the reinforced specimen to that of the unreinforced specimen. In column 7 and 8, aspect ratios and number of reinforcing discs are listed. Interpretation of test results will be considered in the following sections.

1. Failure Strength. The Mohr-Coulomb failure envelope for unreinforced specimens at 12 percent moisture content is plotted in Fig. 39 (tests No. 1-3). Values of cohesion  $c$  and slope of the failure envelope  $\phi$  for these specimens were obtained from figure and are 9 psi. and  $29^\circ$ , respectively. The failure envelope for unreinforced specimens with 17 percent moisture content (tests No. 4-6) is plotted in Fig. 40. Values of cohesion  $c$  and slope of the failure envelope  $\phi$  were obtained from figure and are 5psi. and  $29^\circ$  respectively.

a. Interpretation of Test Results with Enhanced Confining Theory. Mohr's circles and the failure envelope for the reinforced specimens (tests No. 7-9) which have been constructed by using the enhanced confining pressure theory are shown in Fig. 41. In this figure the principal stresses  $\sigma_1$ , at failure were used to construct the Mohr circles tangent to the failure envelope of unreinforced specimens, (tests No. 1-3). Values of enhanced confining pressure ( $\sigma_3 + \Delta\sigma_3$ ) were determined at the intersection point of Mohr circles with the horizontal axis. Failure envelopes for tests No. 10-18 were constructed similarly and are shown in Fig's 42, 43 and 44. Increase in confining pressure  $\Delta\sigma_3$  was then measured for each specimen and are given in Table V. From the table it is clear that in general:

(1) Increases in the confining pressure were approximately the same for tests No. 7-9 and 10-12. This indicates that the change in the moisture content between 12 to 17 percent had little if any effects on the increase in confining pressure,  $\Delta\sigma_3$ .

(2) Increase in the confining pressure decreased by increasing the aspect ratios of the specimens.



b. Interpretation of Test Results with Enhanced Cohesion Theory. Typical Mohr-Coulumb failure envelopes for reinforced specimens (tests No. 7-9 and 10-12) are plotted in Fig. 45 and Fig. 46. These envelopes have been drawn by using the applied confining pressure  $\sigma_3$  and the principal stress at failure  $\sigma_1$ . It is worth mentioning that in a reinforced earth system two modes of failure may occur: (1) Bond stress failure. (2) Reinforcement failure. Strength of the specimen in the former is directly related to the confining pressure, and the bond stress at the soil reinforcement interface is proportional to the effective normal stress. The enhanced cohesion theory leads to dubious results when this mode of failure prevails, as the Mohr's circle is tangential to the curved portion of the failure envelope (refer to Fig. 3, page 10). On the other hand, as the confining pressure increases, a threshold value is reached where the induced shear stress in the reinforcing material reaches its yield strength, after which there is a constant increase  $\Delta\sigma_1$  in the normal stress at failure for a given reinforcing material and spacing. Previous experiments have showed good agreement with the theoretical results for this mode of failure.

In this investigation bond stress failure was the only observed mode of failure for all of the tests performed on the reinforced specimens. Failure occurred at the curved portion of the failure envelope and hence, the enhanced cohesion theory is not applicable in predicting the behavior of the reinforced specimens for confining pressures between 10 to 30 psi.

2. Effects of Moisture Content on Strength of Reinforced Specimens. The strength ratios for reinforced specimens tested at 12 and 17 percent moisture contents and aspect ratio of 0.4 (tests No. 7-9 and 10-12) varied within a narrow range of 2.47 to 2.97. Comparison of the strength ratio for tests No. 8 with 11 and 9 with 12 shows that the strength ratios for the two moisture contents were almost the same. This indicates that increase in the strength ratios was independent of moisture content at range of 12 to 17 percent and the increase in the enhanced confining pressure was similar for the specimens tested under the same confining pressure.

**Table V. VALUES OF ENHANCED CONFINING PRESSURE FROM TEST RESULTS**

| <b>Test No.</b> | <b>Confining Pressure<br/>psi.</b> | <b>Increase in confining<br/>pressure psi.</b> |
|-----------------|------------------------------------|--|
| 7               | 10                                 | 23.5   |
| 8               | 20                                 | 43.0   |
| 9               | 30                                 | 49.1   |
| 10              | 10                                 | 22.4   |
| 11              | 20                                 | 36.9   |
| 12              | 30                                 | 49.1   |
| 13              | 10                                 | 20.4   |
| 14              | 20                                 | 24.3   |
| 15              | 30                                 | 38.0   |
| 16              | 10                                 | 4.6  |
| 17              | 20                                 | 5.7  |
| 18              | 30                                 | 18.3   |

3. Effects of Aspect Ratio on Strength of Reinforced Specimens. Table IV, page 52 indicates that the effect of reinforcement on shear strength decreased with increasing aspect ratio. Nonetheless the strength ratios for both of the specimens with aspect ratios of 2 were almost equal to one, which indicates that for this aspect ratio, reinforcement had no apparent effect on the shear strength.

Surprisingly this is the same aspect ratio at which previous investigations, i. e. Bishop and Green (1965), have showed that the effect of non-lubricated ends on the shear strength of unreinforced specimen was of little significance and the shear strength of lubricated and non-lubricated specimens were about the same.

#### D. EFFECT OF REINFORCEMENT ON MODULUS

Values of tangent moduli, secant moduli at 50 percent of failure stress and secant moduli at 50 percent of failure strain for tests No. 1-15 are given in Table VI.

1. Tangent Modulus. A surprising result is that the tangent moduli of reinforced specimens are smaller than the tangent moduli of unreinforced specimens. This behavior was consistently observed in all tests. It is believed that decrease in tangent moduli of reinforced specimens is due to an initial seating between the soil particles and the reinforcing fabric.

2. Secant Modulus at 50 Percent of Failure Stress. Again the values of secant moduli at 50 percent of failure stress were smaller for unreinforced specimens. This behavior is believed to be due to the much larger strain experienced by the reinforced specimens to reach to 50 percent of maximum failure stress (about 10 times as high as unreinforced specimens).

3. Secant Modulus at 50 Percent of Failure Strain. Conversely, the values of secant moduli at 50 percent of failure strain were larger for reinforced specimens than for unreinforced specimens, Table VI. The values of secant moduli decreased in a consistent rate with increasing aspect ratio.

Table VI. VALUES OF TANGENT AND SECANT MODULUS

| Test No | Tangent modulus<br>psi. | Secant modulus<br>at 50% stress<br>psi. | Secant modulus<br>at 50% strain<br>psi. |
|---------|-------------------------|---|---|
| 1       | 5343                    | 5044                                    | 471                                     |
| 2       | 5024                    | 3467                                    | 904                                     |
| 3       | 8126                    | 4485                                    | 1096                                    |
| 4       | 5020                    | 3761                                    | 460                                     |
| 5       | 4523                    | 3467                                    | 843                                     |
| 6       | 7803                    | 4627                                    | 929                                     |
| 7       | 4970                    | 1261                                    | 807                                     |
| 8       | 4647                    | 1709                                    | 1373                                    |
| 9       | 5093                    | 3576                                    | 1696                                    |
| 10      | 2386                    | 1250                                    | 746                                     |
| 11      | 4397                    | 1567                                    | 1110                                    |
| 12      | 4273                    | 1875                                    | 1417                                    |
| 13      | 4350                    | 1290                                    | 707                                     |
| 14      | 4673                    | 1391                                    | 808                                     |
| 15      | 5767                    | 2104                                    | 1198                                    |
| 16      | 2756                    | 1089                                    | 576                                     |
| 17      | 3480                    | 1394                                    | 679                                     |
| 18      | 4523                    | 1916                                    | 966                                     |

## E. DISCUSSION

Previous investigations have shown that bond stress at the soil reinforcement interface does not reach its maximum value globally as the specimen is subjected to a strain. Indeed in order to mobilize the maximum bond stress, a relative displacement has to occur between the soil and the reinforcement. The magnitude of this displacement depends on properties of both the soil and the reinforcement.

Examining the stress-strain curves of reinforced specimens shows that in general, at a given confining pressure and for strain of less than 1 percent, deviator stresses are smaller for reinforced specimens than deviator stress for unreinforced specimens tested under the same confining pressure. Deviator stresses of reinforced specimens exceeded the deviator stresses of unreinforced specimens when the applied axial strain  $\epsilon_v$  was somewhere between 1 and 2 percent, e. g.  $1 < \epsilon_v < 2$ . Strength of reinforced specimens increased linearly beyond this point and up to failure. This behavior is believed to be due to a non-linear interaction between the soil and the reinforcing fabric and will be explained in the following paragraphs.

As a triaxial specimen is subjected to a compressive stress  $\sigma_v$ , it experiences a lateral strain in the horizontal direction. The magnitude of this lateral strain depends on the Poisson's ratio of the soil and the stiffness of the reinforcing fabric. However, this lateral strain is not uniformly distributed along the cross-section of the specimen, and varies from zero at the center of the specimen to its maximum value at the edge of the specimen. Furthermore the stiffness of the reinforcing fabric is not the same as the stiffness of the soil, and therefore at any given point each one experiences a different strain at the interface. In a conventional reinforced specimen, reinforcing material is stiffer than the soil and at a given point, displacement of the soil in the lateral direction is larger than the displacement of the reinforcing material in the same direction. Hence, a relative displacement takes place at the soil-reinforcement interface and consequently frictional stress is mobilized. The magnitude of the mobilized bond stress increases with increasing strain up to the limiting value of the frictional stress. This limiting value first occurs at the edge of the specimen where the relative displacement between the soil and the reinforcement is the largest. From this point any increase in the strain causes adjacent parts of

the specimen at the interface to reach to the limiting value. This process progressively continues and moves toward the center of the specimen. Therefore increase in the strain has caused a larger portion of the reinforcing fabric to become effective and hence, the strength of the specimen is increased.

1. Comparison of Tests Results With Enhanced Confining Theory. Fig. 47 shows the strength ratios (ratio of reinforced specimen to unreinforced specimen deviator stress) for reinforced specimens with 17 percent moisture content, and subjected to 30psi. (207kPa.) confining pressure, plotted against aspect ratios. Plot of strength ratio versus aspect ratio obtained from equation 3.16 is also shown by the solid line.

The general validity of the proposed enhanced confining model is confirmed by the test results. However, the experimental points lie below the theoretical line. This discrepancy between the test and theoretical results is most probably caused by the following factors:

a. The stiffness of reinforcing fabric is not, as assumed in theory, infinite, compared to the soil stiffness. By applying a compression load to the specimen, a frictional stress is mobilized at the soil-reinforcement interface. Consequently, the reinforcing fabric is put in tension and experiences a strain  $\epsilon_f$ . On the other hand, for the same confining pressure and at a given point, the magnitude of normal stress is larger for specimens with smaller aspect ratios. By assuming that the mobilized frictional stress is proportional to the applied normal stress, then the stress acting on the reinforcing fabric would also be larger. Therefore at a given longitudinal strain, strain in the reinforcing fabric is larger for specimens with a small aspect ratio and hence,  $\epsilon_{fs} > \epsilon_{fl}$ , where  $\epsilon_{fs}$  is the strain in the reinforcement for the specimens with small aspect ratios and  $\epsilon_{fl}$  is the strain in the reinforcement for the specimens with large aspect ratios. If the lateral strain in the soil is  $\epsilon_s$ , then the relative displacement at a given strain at the soil-reinforcement interface is  $(\epsilon_s - \epsilon_{fs})$ , and hence,  $(\epsilon_s - \epsilon_{fs}) < (\epsilon_s - \epsilon_{fl})$ . Therefore for a given longitudinal strain, the relative displacement at the interface is smaller for specimens with a small aspect ratio and hence, a smaller portion of the reinforcing fabric reaches the limiting value of bond stress. This would cause the specimen to fail at a lower normal stress than the predicted value by the theory.

b. Possible effects of pore water pressure on the angle of bond stress has not been considered.

Another important factor affecting laboratory test results is the effect of non-uniform stress distribution. This phenomenon will be studied in more detail in the following section.

2. Effects of Non-uniform Stress Distribution. Inspection of deformations showed that reinforced specimens with aspect ratios of 0.4 and 0.5 deformed rather uniformly along their longitudinal axis, Fig. 48.a, while the specimens with aspect ratios of 0.67 and larger, bulged at mid-height of each reinforced layer, Fig. 48.b. It was further noticed that bulging increased with increasing aspect ratio of the specimen. This indicated the non-uniformity of stress distribution inside the specimens which increased with increasing the aspect ratios of the specimens.

In order to assess the quantitative effect of non-uniform stress distribution on the shear strength of the specimens, it was deemed necessary to calculate the angle of bond stress at the soil-reinforcement interface. Two methods were used in determining this value. In the first method angle of bond stress was back-calculated by assuming a uniform stress distribution in the specimens. By using equation 3.12, page 39, and knowing the values of  $\sigma_1$ , from the test results on reinforced specimens with aspect ratios of 0.4 (tests No. 10-12), the average value of angle of friction was calculated. In this analysis it was assumed that the of angle of bond stress varies linearly along the radius of the specimen as shown in Fig. 49. In the second method the limiting value of the angle of bond stress was calculated by using a relationship proposed by Ingold (1980). He also assumed a linear variation of the angle of bond stress along the radius of the specimen. The values of angle of friction by both methods are in good agreement. The average value of angle of bond stress was  $18^\circ$  by the former method with a scatter of 0.6 and  $19^\circ$  by the latter.

Assessment of the angle of bond stress enables us to predict the effects of non-uniform stress distribution for different aspect ratios and consequently calculate the true values of shear strength of the reinforced specimens. Theoretical values of strength were calculated by the average value of angle of friction ( $19^\circ/2$ ) and equation 3.12, the results are shown in Table VII.

From the table it is clear that non-uniform stress distribution had a significant effect on strength of the specimens specially for aspect ratios of 1 and larger. For aspect ratio of 2, the theoretical values of strength are larger by as much as 27 percent. Hence, it can be concluded that for large aspect ratios non-uniform stress distribution is the main reason for the test results to fall below the theoretical line.

It is worth mentioning that for an aspect ratio of 2, the shear strength of unreinforced and reinforced specimens were almost the same, Table IV, page 40. This indicates that at this aspect ratio the induced strength caused by the reinforcing fabric is totally counteracted by the reduction of strength caused by non-uniform stress distribution within the specimen.

#### F. COMPARISON OF THE BEAM-COLUMN MODEL WITH EXPERIMENTAL DATA

The validity of the proposed Beam-Column model is examined by comparing the theoretical values of normal stress obtained from the proposed Beam-Column model and the experimental results of the normal stress measurements across the mid-height and near the end of the sand specimen tested by Shockley and Ahlvin (1960).

Descriptions of the specimens have been given on page 27. Equation 3.16 is used in calculating the values of normal stress across the mid-height of the specimen by assuming that:

- a. An average friction angle of 5 degree at the soil-end platen interface.
- b. Medium dense sand was used, therefore the angle of internal friction of 35 degrees was used.
- c. A central angle of 3 degrees for the sections.

Analytical results are shown by the dotted lines in Fig. 50. Distribution of normal stress across the mid-height is shown in Fig. 50.a. Similarly distribution across the end is shown in Fig. 50.b. The proposed normal stress distributions by Shockley and Ahlvin for the same cross-sections are shown by the solid lines. The figures show the general validity of the model for stress distribution at the mid-height and top of the specimen. The analytical values are in good agreement with the theory inasmuch as:



a. Maximum normal stress at the mid-height occurs at the center line of the specimen and is equal to 38.2 psi.

b. Minimum normal stress at the mid-height occurs at the edge of the specimen and is equal to 25.9 psi.

c. Maximum normal stress at the end of specimen occurs at the edge of the specimen and is equal to 34.1 psi.

d. Minimum normal stress at the end of specimen occurs at the center line of the specimen and is equal to 21.7 psi.

**Table VII. THEORETICAL STRENGTH BASED ON ENHANCED CONFINING THEORY**

| Test No | Aspect Ratio | Theoretical Deviator Stress psi. | Strength Ratio | Theo./lab. Strength |
|---------|--------------|----------------------------------|----------------|---------------------|
| 12      | 0.40         | 240.9                            | 3.10           | 1.12                |
| 15      | 0.50         | 177.8                            | 2.29           | 1.15                |
| 18      | 0.67         | 138.1                            | 1.78           | 1.10                |
| 19      | 1.00         | 111.7                            | 1.44           | 1.20                |
| 21      | 2.00         | 92.3                             | 1.19           | 1.27                |

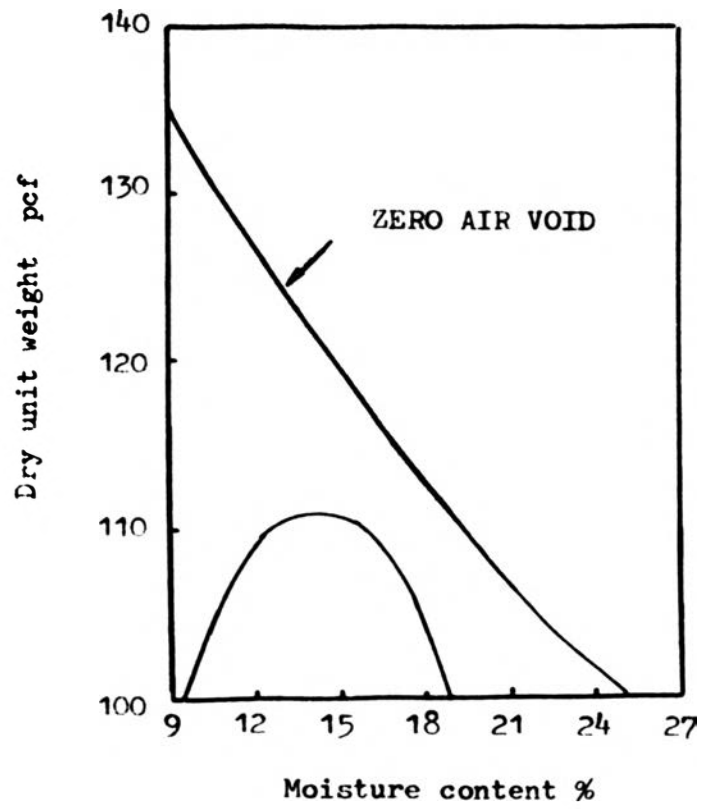


Figure 32. Compaction curve.

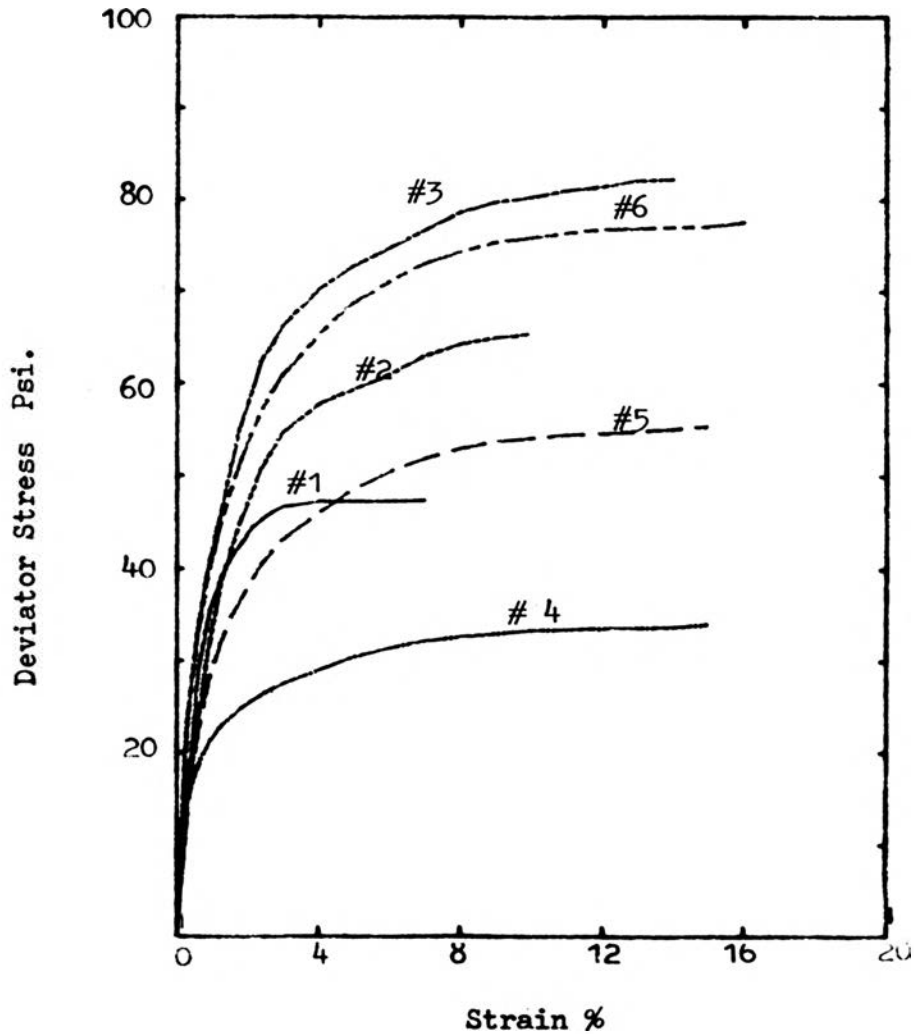


Figure 33. Stress-strain relationship for unreinforced specimens. Tests No. 1, 2 & 3 at 12% moisture content and tests No. 4, 5 & 6 at 17% moisture content.

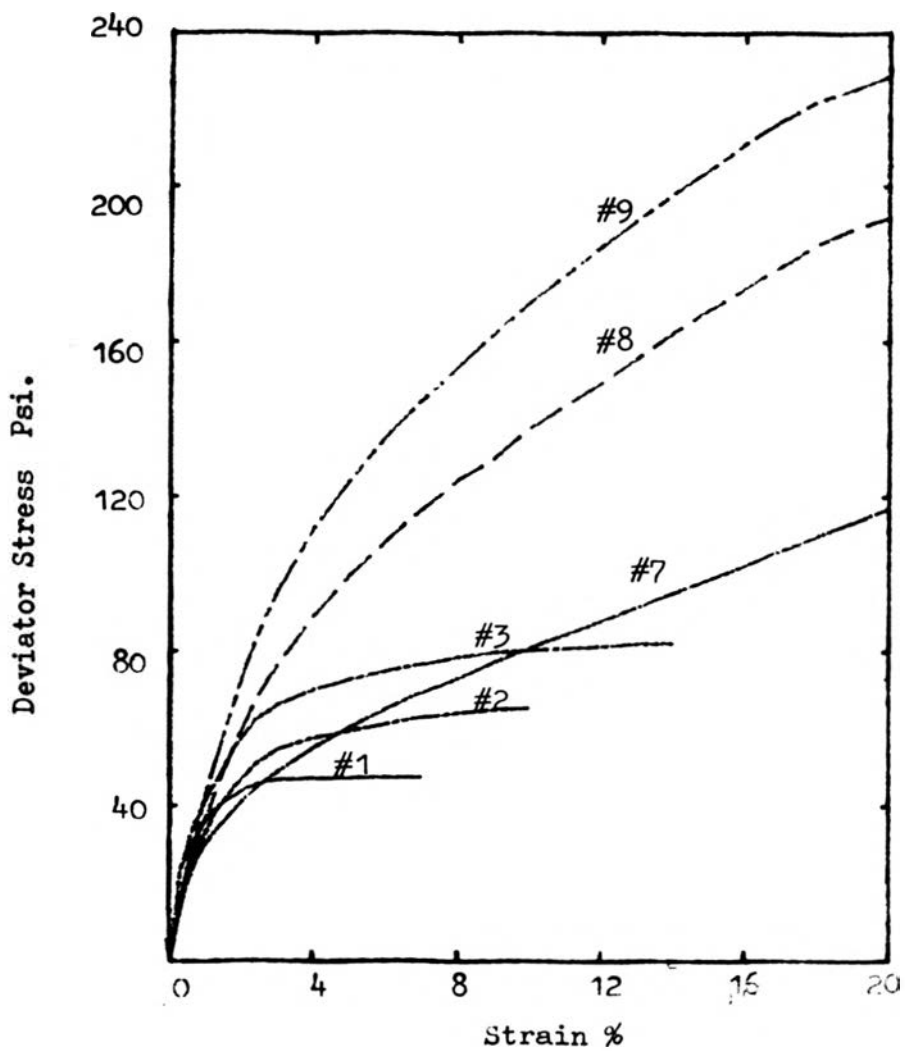


Figure 34. Stress-strain relationship for reinforced specimens with aspect ratio of 0.4 and 12% moisture content. Tests No. 7, 8 & 9, compared with Tests No. 1-3.

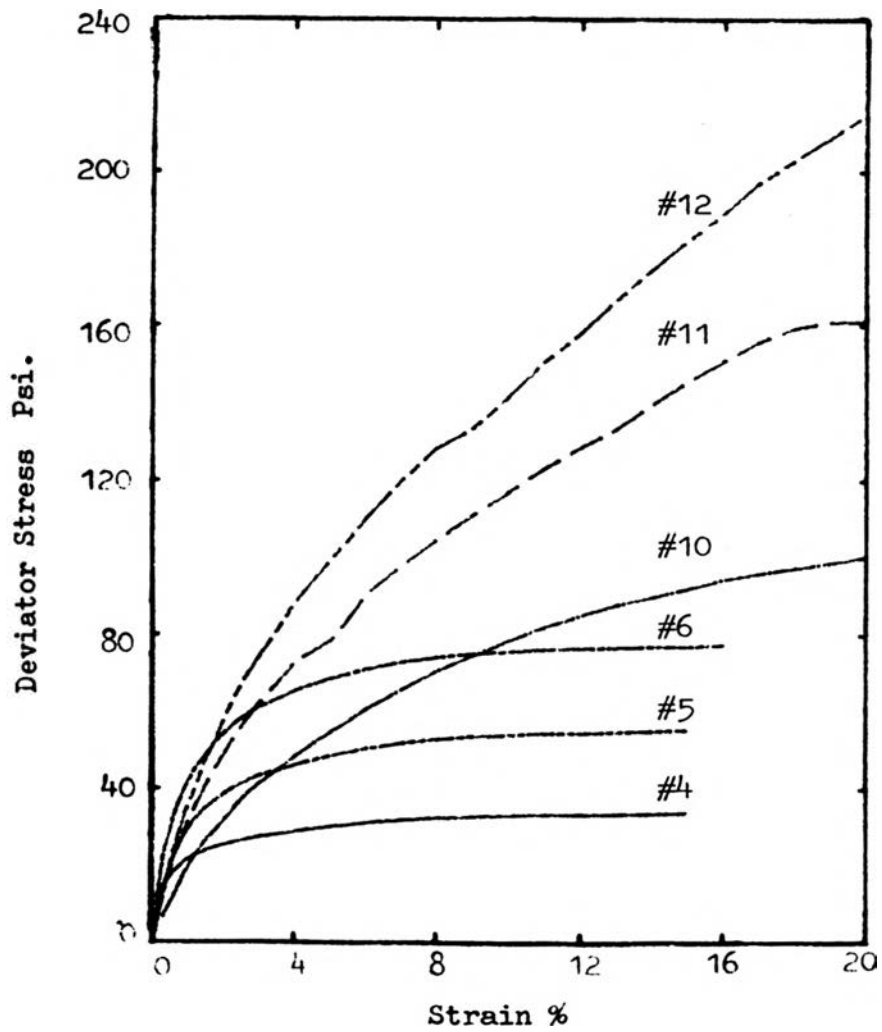


Figure 35. Stress-strain relationship for reinforced specimens with aspect ratio of 0.4 and 17% moisture content. Tests No. 10, 11 & 12, compared with tests No. 4-6.

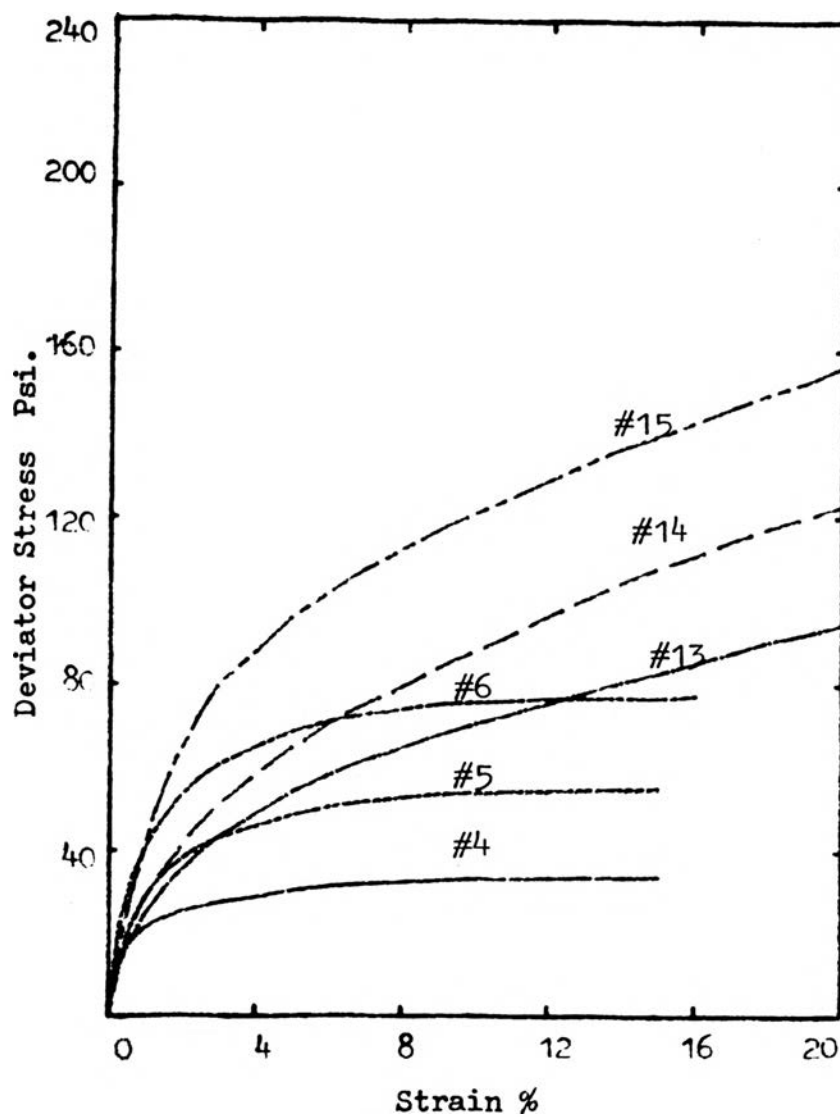


Figure 36. Stress-strain relationship for reinforced specimens with aspect ratio of 0.5 and 17% moisture content. Tests No. 13, 14 & 15, compared with tests No. 4-6.

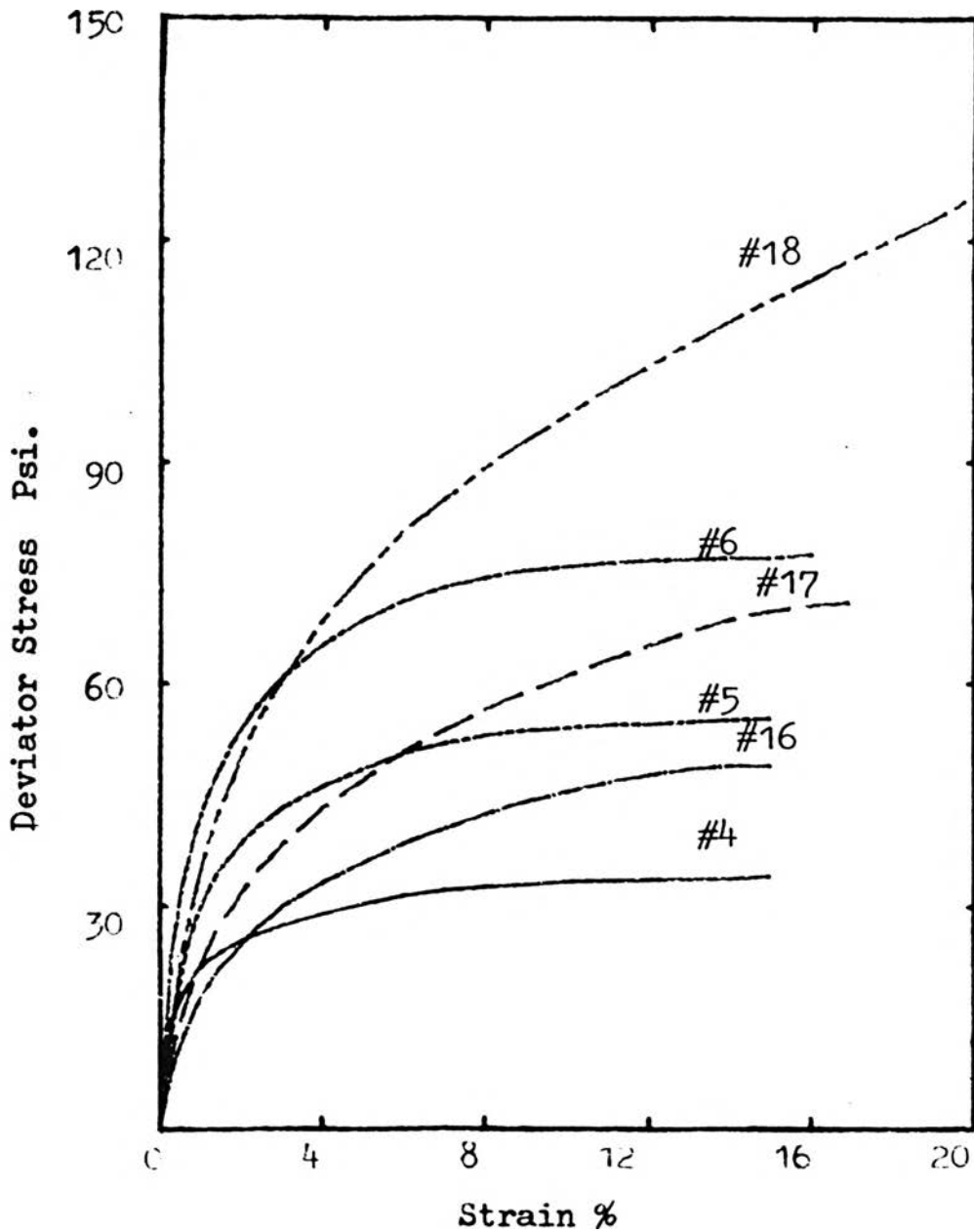


Figure 37. Stress-strain relationship for reinforced specimens with aspect ratio of 0.67 and 17% moisture content. Tests No. 16, 17 & 18, compared with tests No. 4-6.



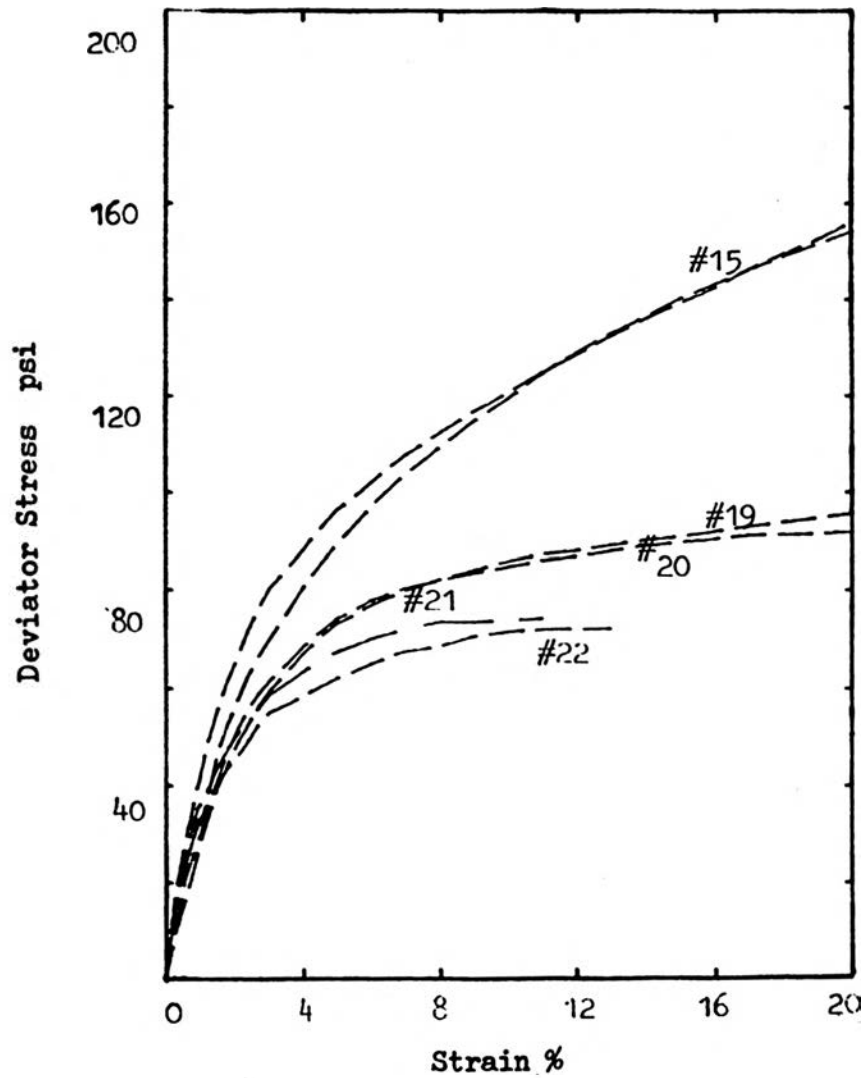


Figure 38. Comparison of stress-strain curves for 3 pairs of identical tests. No. 15, 20, 21, 22 & 23.

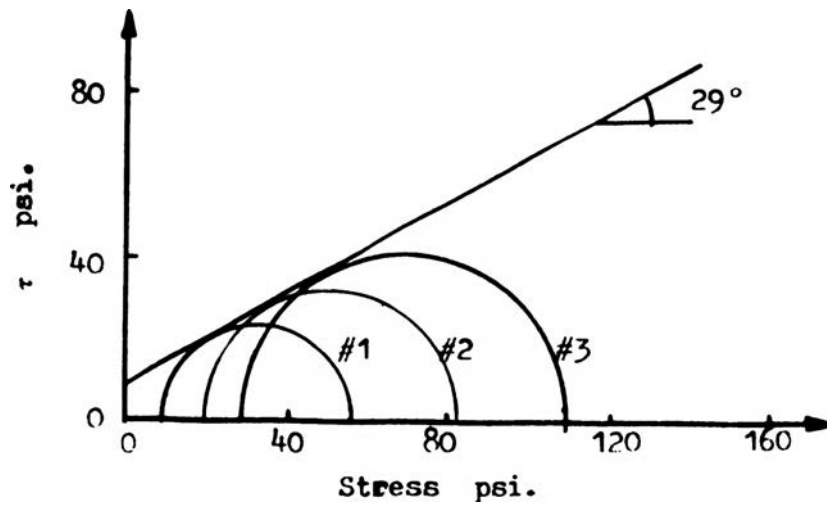


Figure 39. Mohr-Coulomb failure envelope for unreinforced specimens with 12% moisture content, tests No. 1-3.

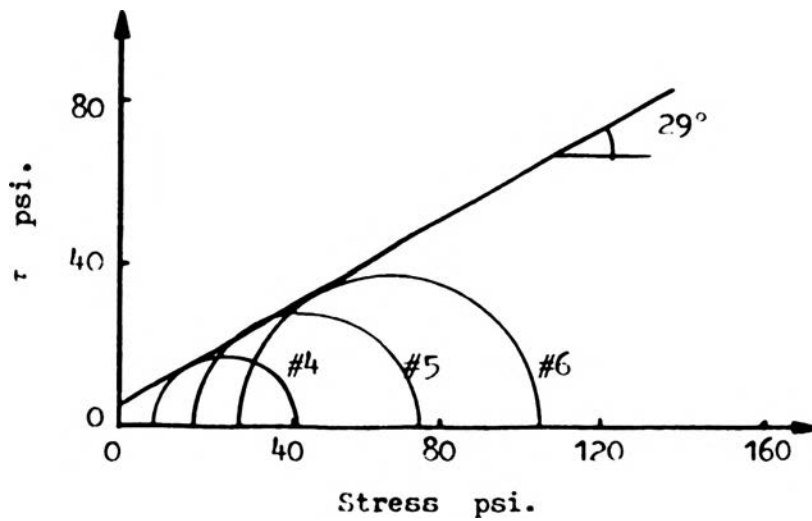


Figure 40. Mohr-Coulomb failure envelope for unreinforced specimens with 17% moisture content, tests No. 4-6.

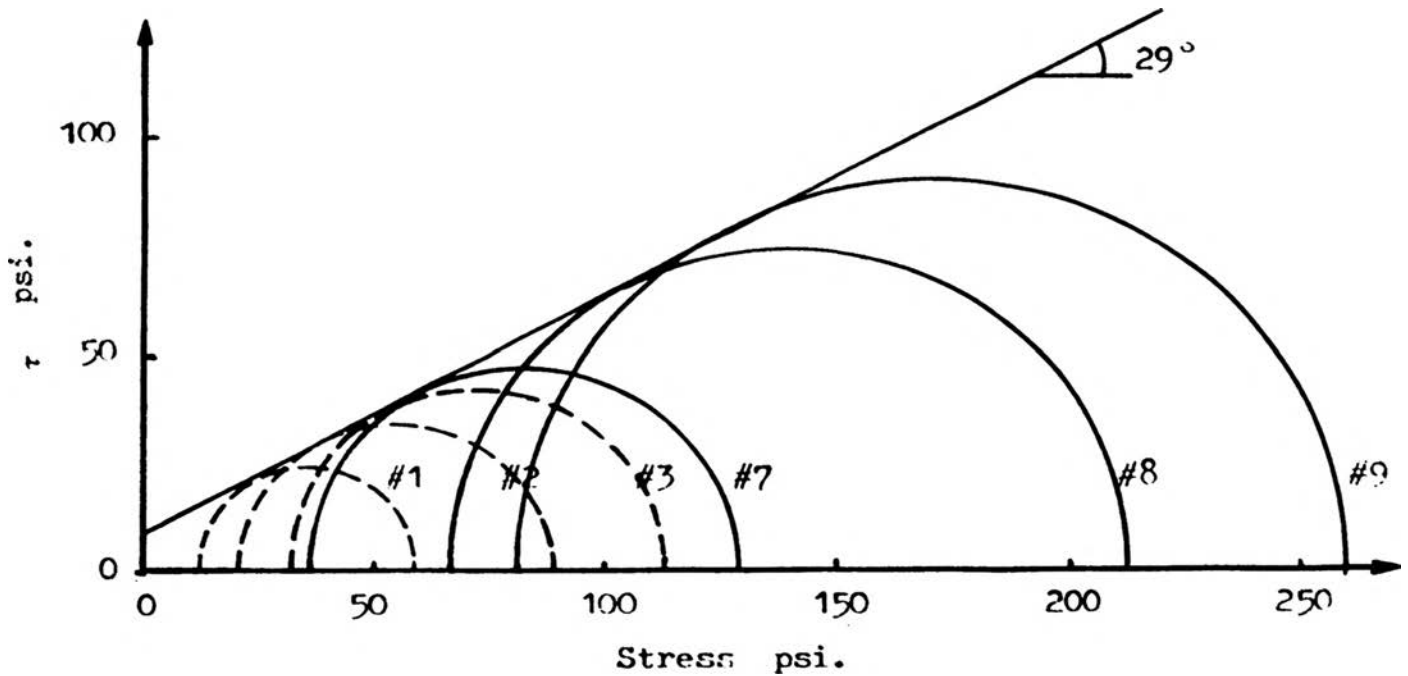


Figure 41. Mohr-Coulomb failure envelope for tests No. 7-9, using the enhanced confining pressure theory, compared with tests No. 1-3.

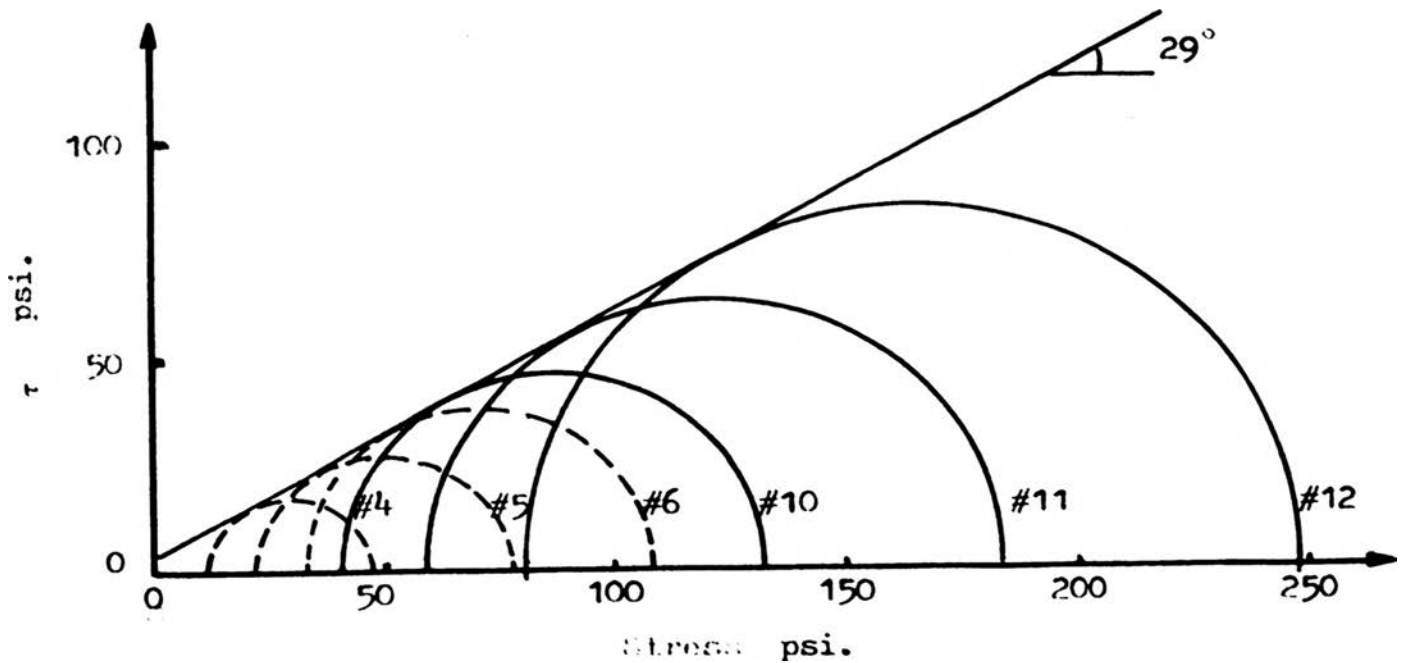


Figure 42. Mohr-Coulomb failure envelope for tests No. 10-12, using the enhanced confining pressure theory, compared with tests No. 4-6.

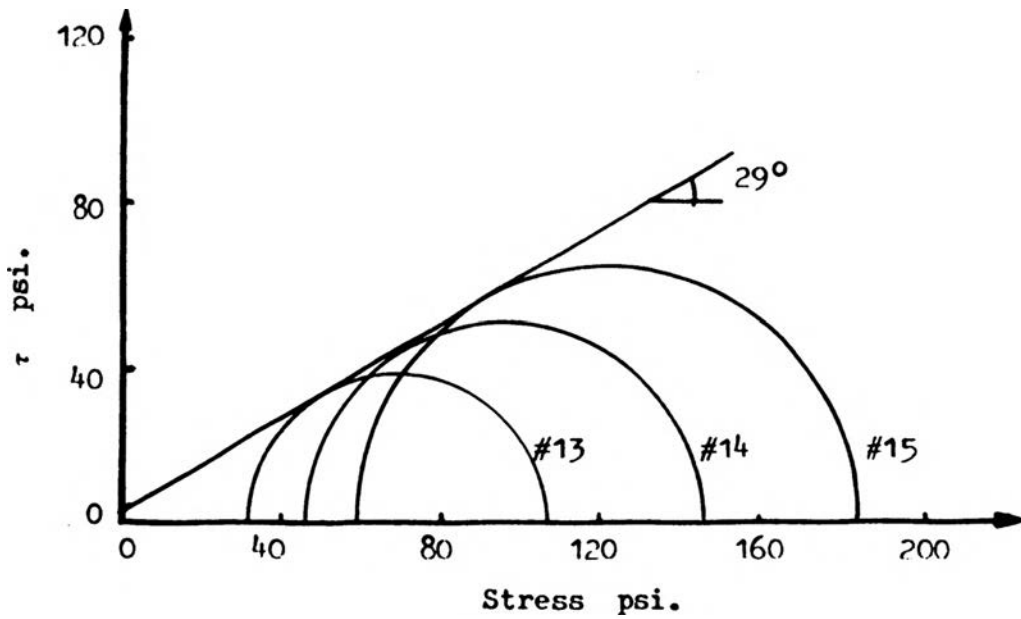


Figure 43. Mohr-Coulomb failure envelope for Tests No. 13-15, using the enhanced confining pressure theory.

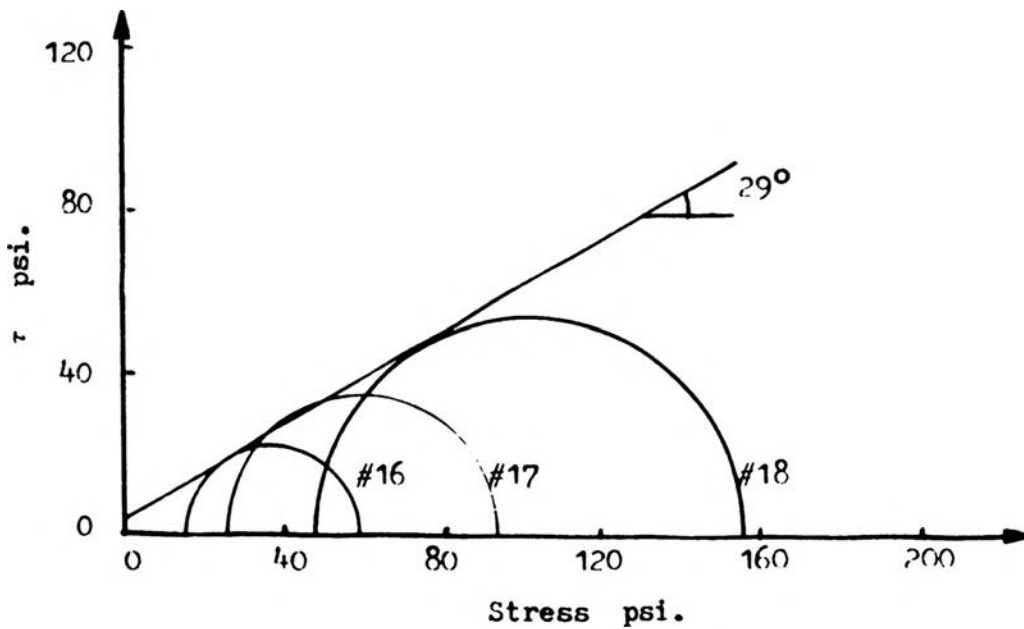


Figure 44. Mohr-Coulomb failure envelope for tests No. 16-18, using the enhanced confining pressure theory.

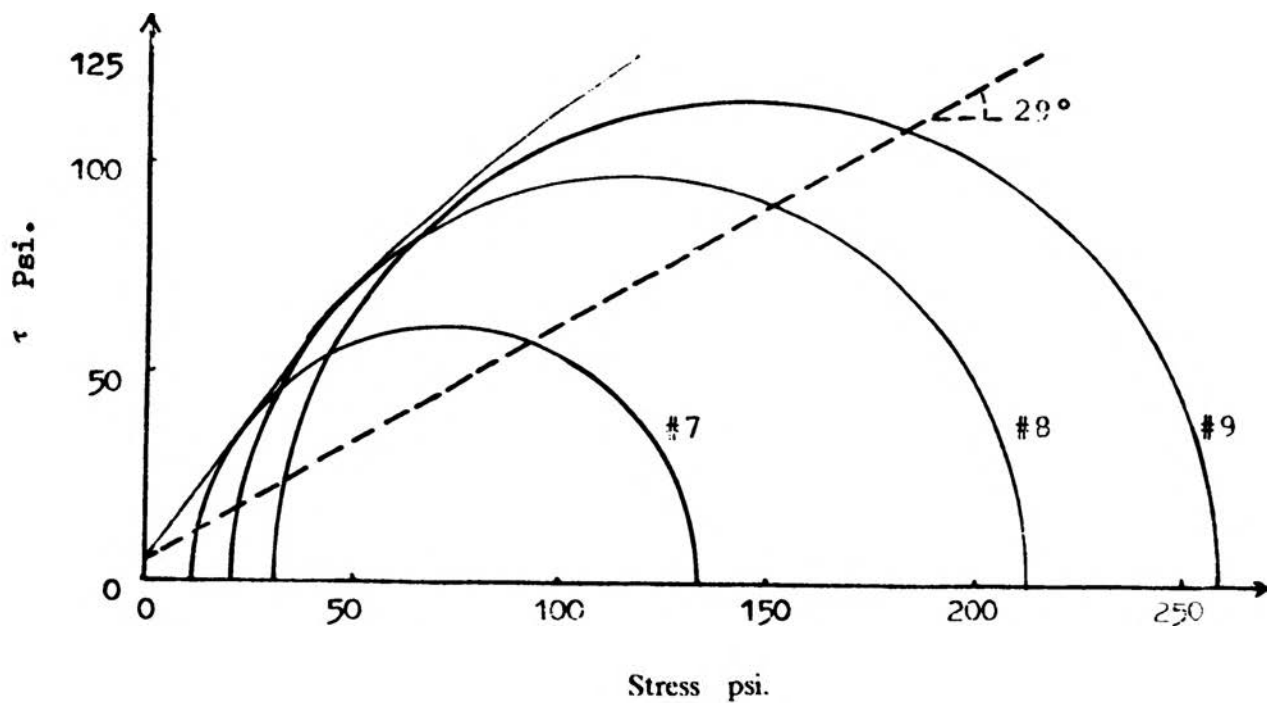


Figure 45. Mohr-Coulomb failure envelope for tests No. 7-9, using enhanced cohesion theory.

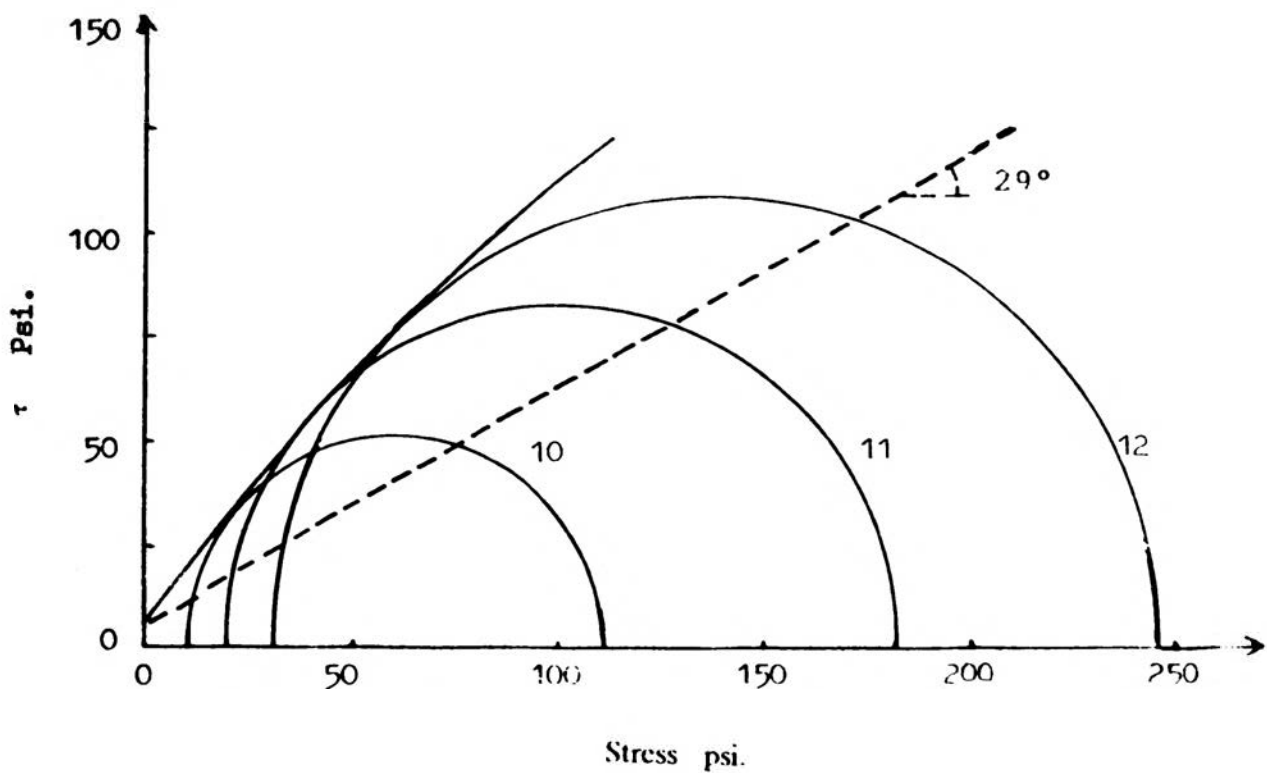


Figure 46. Mohr-Coulomb failure envelope for tests No. 10-12, using enhanced cohesion theory.

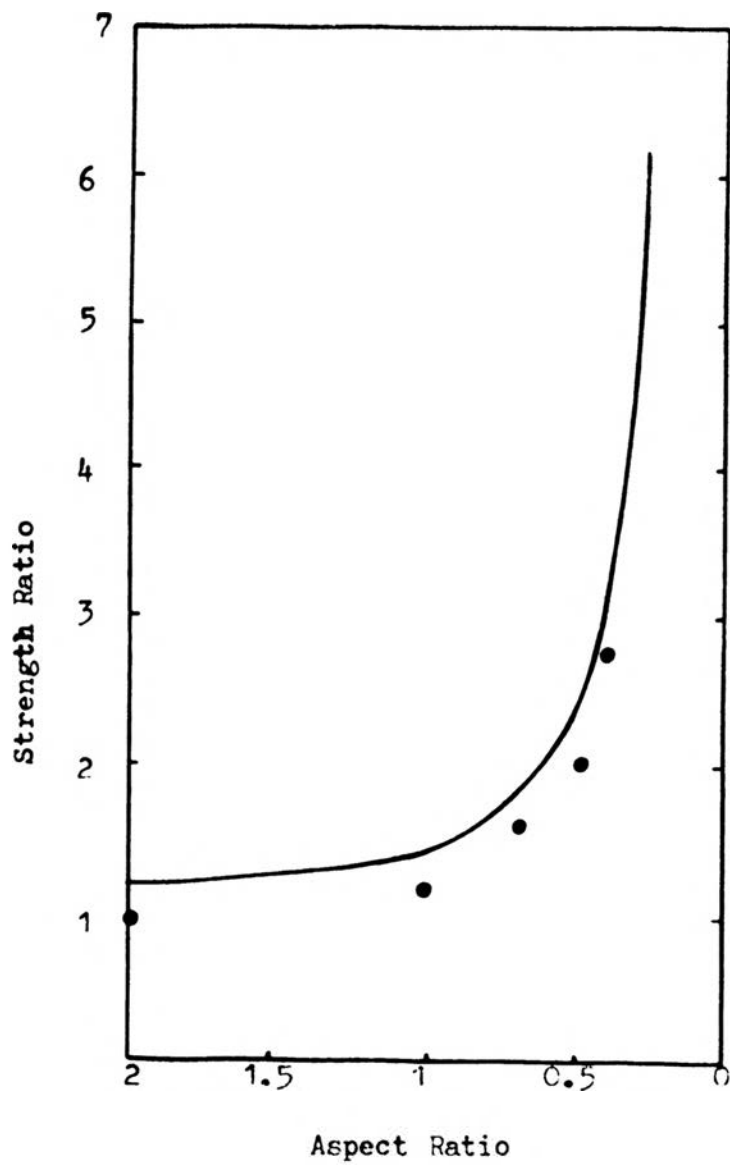


Figure 47. Comparison of the experimental with theoretical results based on the enhanced confining pressure theory.

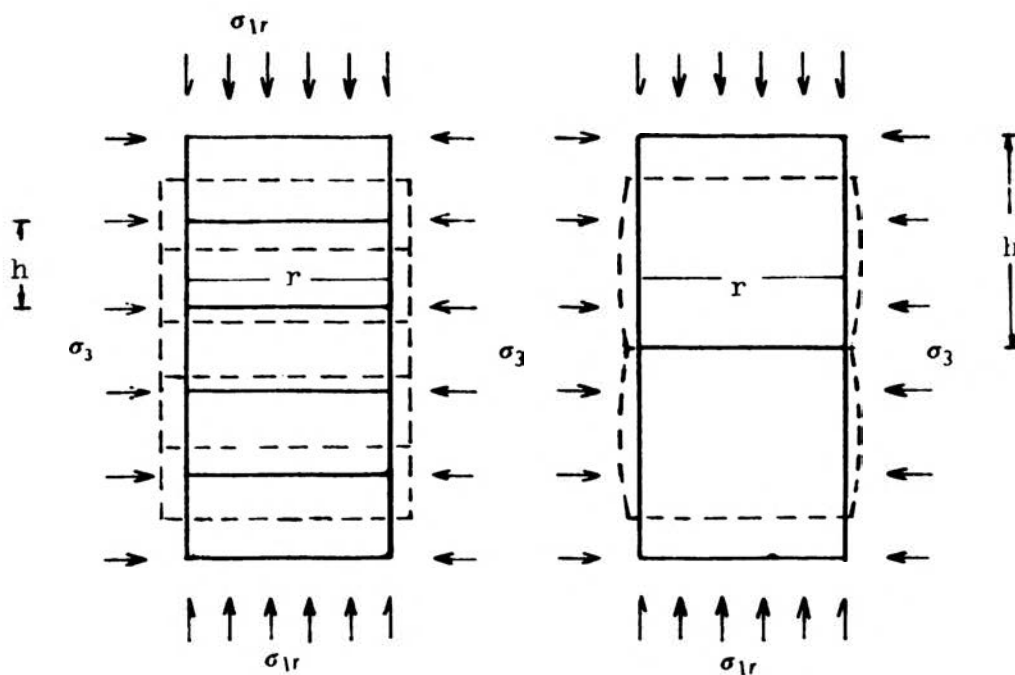


Figure 48. Comparison of the experimental with theoretical (b) for aspect ratios  $> 0.67$ .

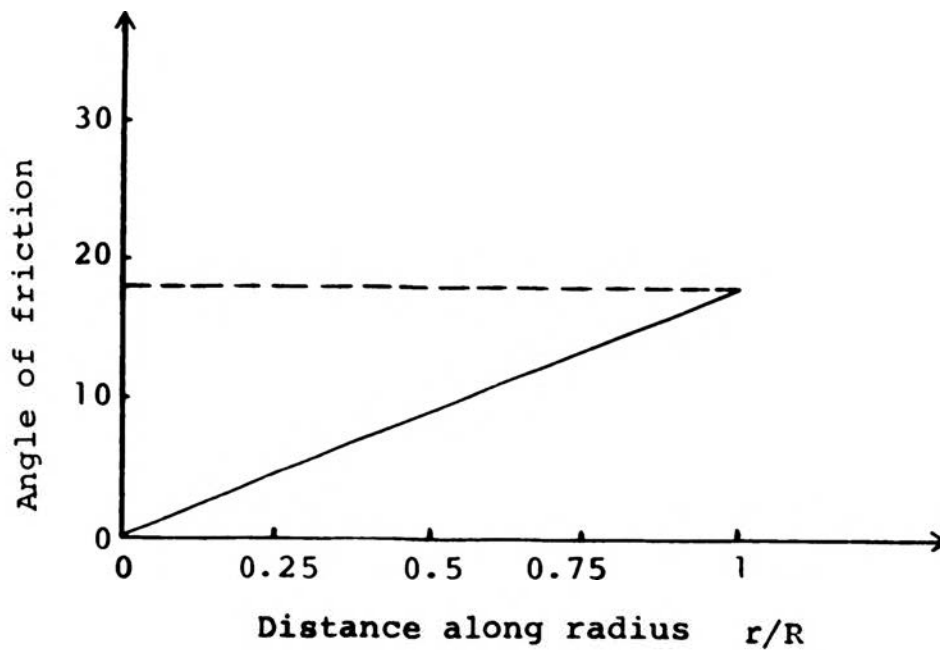


Figure 49. Variation of bond stress angle along radius.

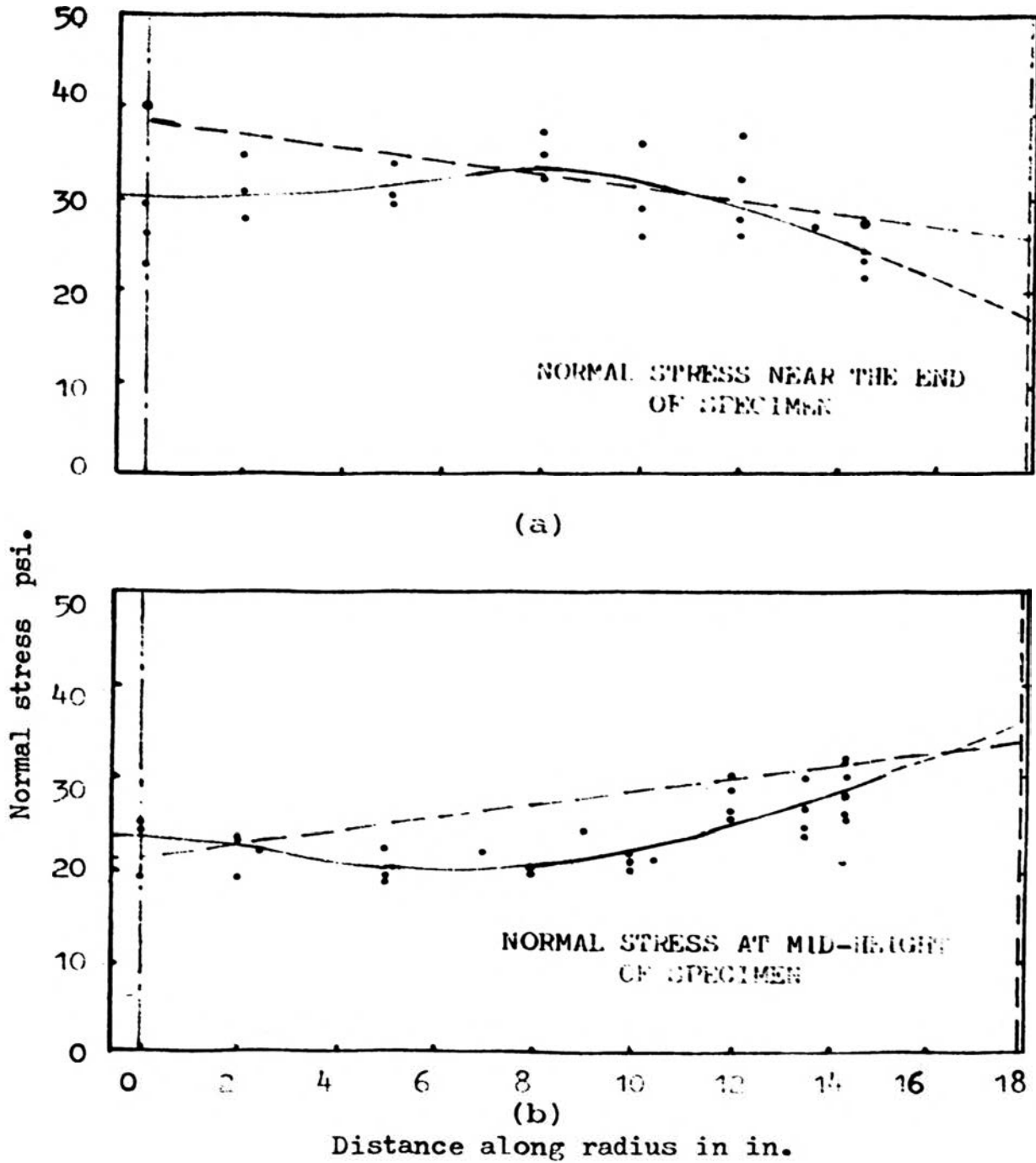


Figure 50. Comparison of experimental and theoretical values of normal stress: a- across the mid-height, b- across the end.



## V. CONCLUSIONS

Soil-reinforcement exhibits a complex phenomenon derived from non-linear interaction between soil particles and reinforcing fabric. This complexity is increased when considering the behavior of reinforced triaxial specimens by non-uniform stress and strain distribution generated within them.

In order to calculate the effect of reinforcement on shear strength of reinforced triaxial specimens a modified analytical model based on the enhanced confining pressure theory is developed. The proposed model can also be used for calculating the effect of rough end platens on strength of unreinforced cylindrical specimens.

The effects of non-uniform stress distribution on strength of unreinforced and reinforced triaxial specimens were considered. A new model based on the Beam-Column analogy is developed which can be used in predicting the effects of end friction on stress distribution and strength of both reinforced and unreinforced specimens.

Despite the uncertainties, encouraging results were obtained during the course of this investigation. From theoretical and experimental results, the following conclusions were made:

1. Reinforcing of unsaturated loess specimens with a woven fabric increased its shear strength by as much as 300 percent for an aspect ratio of 0.4.
2. The reinforced loess specimens experienced large strain in order to develop their maximum strength.
3. Strength ratios were insensitive to variation of moisture contents between 12 and 17 percent.
4. The shear strength of reinforced specimens are inversely related to the aspect ratios.
5. Specimens with aspect ratios of 0.5 and smaller deformed uniformly along their longitudinal axis, indicating that strain and stress are more or less uniformly distributed within these specimens. On the other hand, for specimens with aspect ratios of 0.67 and larger, deformation was accompanied by bulging of the specimen at the mid-height of each reinforced soil layer. Bulging of the specimens increased with increasing aspect ratio, which indicated that the non-uniform stress distribution within the specimens increased.

6. Non-uniform stress distribution reduced the strength of reinforced specimens with aspect ratios of 2 by as much as 27 percent.
7. Tangent moduli of reinforced specimens were smaller than of unreinforced specimens. Secant moduli at 50 percent of failure stress were also smaller for reinforced specimens.
8. However, secant moduli at 50 percent of failure strain were larger for reinforced specimens. At a given confining pressure values of secant moduli at 50 percent of strain decreased with increasing aspect ratio.
9. At the present time it is impractical to draw a direct correlation between laboratory test results and behavior of reinforced loess structures in the field.
10. The stiffness and secant modulus of the reinforcing fabric are two important properties of reinforcing material, which should be considered in designing reinforced earth structures.
11. Theoretical results based on the Beam-Column method showed good agreement with the normal stress distribution measured at the mid-height and near the end of a 70in long sand specimen tested by Shockley and Ahlvin.

## REFERENCES

1. Al-Chalabi, M. (1973), "Stress Distribution Within Circular Cylinders in Compression," Ph. D Dissertation, Kansas State University, 1973.
2. Al-Chalabi, M., and Huang, C.L., (1974), "Stress Distribution within Cylinders in Compression," *Int. J. Rock Mech. Min. Sci. Geomech. Abstr.* Vol. 11, 1974, pp. 45-56.
3. Balla, A. (1960), "A New Solution of The Stress Conditions in Triaxial Compression," *Acta. Tech. Hung.* 28, 1960, pp. 349-387.
4. Balla, A. (1960), "Stress Condition in Triaxial Compression Test," 4th Int. Conference in Soil Mechanics and Foundation Engineering, Vol. 1, 1960, pp. 140-143.
5. Barden, L. and McDermott, R. J. W. (1965), "Use of Free Ends in Triaxial Testing of Clays," *J. of Soil Mechanics and Foundation Engineering, ASCE*, Vol. 91, No. SM6, Nov. 1965, pp. 1-23
6. Bishop, A. W. and Green, G. E. (1965), "The Influence of End Restraint on the Compression Strength of a Cohesionless Soil," *Geotechnique*, 15-3 (1965), pp.243-266.
7. Blight, G. E. (1965), "Shear Stress and Pore Pressure in Triaxial Testing," *J. of the Soil Mechanics and Foundation Division. ASCE*, Vol. 91, No. SM6, Nov. (1965), pp. 25-39.
8. Bouvard, D. and Stutz, S. (1986), "Experimental Study of Rheological Properties of a Sand Using a Special Triaxial Apparatus," *Geotechnical Testing J. ASCE* Vol. 9, No. 1, March 1986, pp. 10-18.

9. D'Appolinia, E. and Newmark, N. M. (1951), "A Method for Solution of the Restrained Cylinder Under Compression," Proc. of the First U. S. National Congress Of Applied Mechanics, 1951, pp. 217-226.
10. Filon, I. N. G. (1902), "On the Elastic Equilibrium of Circular Cylinders under Certain Practical Systems of Load", Philosophical Transactions, Royal Society, Series A, Vol. 198, London, 1902. pp. 147-233.
11. Gerrard, C. M. (1981), "Reinforced Soil: An Orthorhombic Material," J. of the Geotechnical Engineering Division, ASCE, Vol. 108, No. GT11, 1981, pp. 1460-1474.
12. Girjavallabhan, C. V. (1970), "Stress in Restrained Cylinder Under Axial Compression", J. of Soil Mechanics and Foundation Division, ASCE, Vol. 96 No. SM 2, March 1970, pp. 783-787.
13. Girjavallabhan, C. V. and Reese, L. C. (1968), "Finite-Element Method for Problems in Soil Mechanics", Journal of Soil Mechanics and Foundation Division, ASCE, Vol. 94 No. SM 2, March 1968, pp. 473-496.
14. Harrison, W. J., and Gerrard, C. M. (1972), "Elastic Theory Applied to Reinforced Earth," J. of the Soil Mechanics and Foundation Division, ASCE, Vol. 98, No. SM12, Dec. 1972, pp. 1325-1346.
15. Herrmann, L. R. and Al-Yassin, Z. (1978), "Numerical Analysis of Reinforced Soil Systems," Proc. of Symposium on Earth Reinforcement, ASCE Annual Convention, Pittsburgh, Pennsylvania, April 1978, pp. 428-457.
16. Hausmann, M. R. (1976), "Strength of Reinforced Soil," Proc. 8th Australian Road Resh. Conf. Vol. 8, 1976, pp. 1-8.

17. Ingold, T. S. (1979), "Reinforced Clay-A Preliminary Study Using the Triaxial Apparatus," Proc. of Int. Conference on Soil Reinforcement, Vol. 1. Paris, 1979, pp. 59-64.
18. Ingold, T. S. (1980), "Reinforced Clay", Ph. D. thesis, University of Surrey, at Guilford, England (1980).
19. Ingold, T. S. (1981), "A Laboratory Simulation of Reinforced Clay Walls," Geotechnique, 31, No. 3, 1981, pp. 399-412.
20. Ingold, T. S. and Miller, K. S. (1982), "Analytical and laboratory Investigation of Reinforced Clay", Proc. of the Second Int. Conference on Geotextiles, Industrial Association Int., Vol 3, Aug., 1982, pp. 587-592.
21. Ingold, T. S. and Miller, K. S. (1982), "The Behavior of Geotextile Clay Subjected to Undrained Loading," Proc. of the Second Int. Conference on Geotextiles, Industrial Association Int., Vol 3, Aug., 1982, pp. 593-597.
22. Jewell, R. A. (1980), "Some Effect of Reinforcement on the Material Behavior of Soils", Ph. D. thesis, University of Cambridge, Cambridge, England, 1980.
23. Jewell, R. A. and Janes, C. J. F. P. (1981), "Reinforcement of Clay Soils and Waste Materials Using Grids," Proc. of the 10th Int. Conference on Soil Mech. and Foundation Engineering. Vol. 3 Stockholm, Jun. 1981, pp. 701-706.
24. Jones, C. J. F. P. (1978), "The York Method of Reinforced Earth Construction," Proc. of Symposium on Earth Reinforcement, ASCE Annual Convention, Pittsburgh, Pennsylvania, April, 1978, pp. 501-527.

25. Juran, I. and Schlosser, F. (1978), "Theoretical Analysis of Failure in Reinforced Earth Structures," Proc. of Symposium on Earth Reinforcement, ASCE Annual Convention, Pittsburgh, Pennsylvania, April, 1978, pp. 528-555.
26. Kirkpatrick, W. M. and Belshaw, D. J. (1968), "On the Interpretation of the Triaxial Test", *Geotechnique*, Vol. 18, No. 3, Sep. 1968, pp. 336-350
27. Kirkpatrick, W. M. and Younger, J. S. (1970), "Strain Conditions in Compression Cylinder," *J. of the Soil Mechanics and Foundation Division, ASCE*, Vol. 96 No. SM5, Sep. 1970, PP. 1683-1695.
28. Lee, K. I.. (1978), "Mechanisms, Analysis and Design of Reinforced Earth," Proc. of Symposium on Earth Reinforcement, ASCE Annual Convention, Pittsburgh, Pennsylvania, April 27, 1978, pp. 62-76.
29. Long, N. T., Gueuan, Y., and Legeay, G., (1972), " Etude de la Terre Armee a l'appareil Triaxial," *Rapport de Recherche*, No. 17, LCPC. Quoted from reference 18.
30. Munster A. (1930), United State Patent Specification No. 1762343.
31. Murray, R. T. and Boden, J. B. (1979), "Reinforced Earth Wall Constructed With Cohesive Fill," Proc. of Int. Conference on Soil Reinforcement, Vol. 2. Paris, 1979, pp. 569-577.
32. Osman, M. (1979), "Energy Method Applied to Soil Reinforcement," Int. Conference on Soil Reinforcement, Vol. 1, Paris, Mar. 20-22, 1979, pp. 108-112.
33. Ottosen, N. S. (1984), "Evaluation of Concrete Cylinder Test Using Finite Elements", *J. Engineering Mechanics*, Vol. 110, No. 3, March 1984, pp. 465-481.

34. Pasley, C. W. (1822), "Experiments on Revetments," John Murray, Vol. 2 London, England, 1822.
35. Peng, S. D. (1971), "Stresses Within Elastic Circular Cylinders Loaded Uniaxially and Triaxially," *Int. J. Rock Mech. Min. Sci.*, 8, 1971, pp. 399-432.
36. Perloff, W. H. and Pombo, L. E., (1969), "End Restraint Effects in the Triaxial Testing of Clay," 7th Int. Conference in Soil Mechanics and Foundation Engineering, Vol. 1, Mexico, 1969, pp. 327-333.
37. Pickett, G. (1944), "Application of Fourier Method to the Solution of Certain Boundary Problems in the Theory of Elasticity", *J. of the Applied Mechanics*, ASME, Vol. 11, September 1944, pp. 176-182.
38. Pietruszczak, S. and Mroz, Z. (1980), "Numerical Analysis of Elastic-Plastic Compression of Pillars Accounting for Material Hardening and Softening," *Int. J. Rock Mech. Min. Sci. Geomech. Abstr*, Vol. 17, 1980, pp. 199-207.
39. Rankilior P. R. (1981), "Membrances in Ground Engineering," John Wiley&Sons I.td. 1981.
40. Razania, R., and Behpour, I. (1970), "Some Studies on Improving the Properties of the Earth Materials used for construction on Rural Houses in Seismic Regions of Iran," *Proc. of the Roorkee Confrence on Earthquake Engineering*, 1970, pp. 82-29.
41. Rowe, P. W. and Barden, L. (1964), "Importance of the Free Ends in Triaxial Testing," *J. of the Soil Mechanics and Foundation Division*, ASCE, Vol. 90, No. SM1, Jan. 1964, pp. 1-27.

42. Sanaith, M. S., Bell, A. L. and Dubois, D. D. (1979), "Embankment Construction from Marginal Material," Proc. of Int. Conference on Soil Reinforcement, Vol. 1, Paris, 1979, pp. 175-180.
43. Saxena, S. K. and Wong, Y. T., (1984), "Frictional Characteristics of a Geomembrane," Int. Conference on Geomembranes, Denver, U.S.A. 1984, pp. 187-190.
44. Schlosser, F., and Long, N. T., (1973), "Etude du Comportement du Matériau Terre Armée," Annales del Institut Technique du Batiment et des Travaux Poblics, Supplement No. 304 Serie Materiaux No. 45.
45. Schlosser, F., and Vidal, H. (1969), "Laterre Armee," Bull. de Liaison LRPC, No. 41, Nov. 1969, pp. 101-144.
46. Schlosser, F., and Long, N. T. (1974), "Recent Results in French Research on Reinforced Earth," J. of the Construction Division, ASCE, Vol. 100, No. CO3, Sep. 1974, pp. 223-236.
47. Scott, R. F., (1985), "Plasticity and Constitutive Relations in Soil Mechanics," J. of Geotechnical Engineering, ASCE, Vol. 111, No. SM5, May. 1985, PP. 563-605.
48. Shockley, W. G. and Ahlvin, R. G. (1960), "Non-Uniform Conditions in Triaxial Test Specimens," ASCE Research Conference on Shear Strength of Cohesive Soils, June 1960, pp. 341-357.
49. Tarzaghi, K. and Peck, R. B., (1948), "Soil Mechanics in Engineering Practice," John Wiley & Sons Inc., New York, 1967



50. Totsuoka, F. and Haibara, O. (1985), "Shear Resistance Between Sand and Smooth or Lubricated Surfaces," *Soils and Foundations*. Vol. 25, No. 1, Mar. 1985, pp. 89-98.
51. Vidal H. (1966), "Technique Du Batiment et des Travaux Public," *La Terre Arme*e Annales Del'Institut, Supplement Vol. 19, No. 223-224, Serie Materiaux 30, 1966.
52. Westergaard, H. M. (1938), "A Problem of Elasticity by a Problem in Soil Mechanics," *Mechanics of Solids, Timoshenko 60th Anniversary*, Macmillan & Co., New York, N. Y., 1938.
53. Wordle, L. J., and Gerrard, C. M., (1972), "the Equivalent Anisotropic properties of Layered Rock and Soil Masses," *Rock Mechanics*, Vol. 4, 1972, pp. 249-259.
54. Yang, z. (1972), "Strength and Deformation Characteristics of Reinforced Sand," Ph. D. Thesis, UCLA, 1972.

## VITA

Mohammad Taghi Izadi was born on Sep.-23-1950, in Shiraz, Iran. He received his primary and secondary education in Shiraz, Iran. He has received his Bachelor of Science degree in Engineering from Southern Illinois University-Edwardsville, Ill. in Aug. 1978. From 1979 to 1985 he worked as a site and design engineer in Iran. He then attended the Graduate school of Southern Illinois University- Edwardsville, in Edwardsville in Fall 1985. He came to the University of Missouri, Ralla in Jan. 1986.